Novel CRITR-seq approach reveals influenza transcription is modulated by NELF and is a key event precipitating an interferon response

Alison C. Vicary[1], Sydney N.Z. Jordan[1], Marisa Mendes[1], Sharmada Swaminath[1], Lennice K. Castro[1], Justin S. Porter[1], Alistair B. Russell[1#]

[1]Department of Molecular Biology, School of Biological Sciences, University of California, San Diego, 9500 Gilman Drive, La Jolla, CA 92093, USA

[#]To whom correspondence should be addressed (a5russell@ucsd.edu)

Summary

Transcription of interferons upon viral infection is critical for cell-intrinsic innate immunity. This process is influenced by many host and viral factors. To identify host factors that modulate interferon induction within cells infected by influenza A virus, we developed CRISPR with Transcriptional Readout (CRITR-seq). CRITR-seq is a method linking CRISPR guide sequence to activity at a promoter of interest. Employing this method, we find that depletion of the Negative Elongation Factor complex increases both flu transcription and interferon expression. We find that the process of flu transcription, both in the presence and absence of viral replication, is a key contributor to interferon induction. Taken together, our findings highlight innate immune ligand concentration as a limiting factor in triggering an interferon response, identify NELF as an important interface with the flu life cycle, and validate CRITR-seq as a tool for genome-wide screens for phenotypes of gene expression.

Introduction

Transcription of type I and type III interferons is one of the first host responses to viral infection in vertebrates and is critical for controlling viral spread.[1,2] Through autocrine and paracrine signaling, interferon secreted from infected cells induces transcription of a set of interferon-stimulated genes (ISGs) that establish an antiviral state in neighboring cells. Innate and adaptive immune cells also respond to interferon signaling, promoting a systemic immune response[3].

Only a small fraction of infected cells successfully detect viral infection and produce interferons[4–8]. For example, wild-type influenza A virus (IAV) induces interferon expression in less than 1% of cells infected in tissue culture[9]. Although this fraction of responders is small, paracrine signaling allows these few interferon-producing cells to have a critical protective effect[10]. Demonstrating the importance of this pathway for effective viral clearance, mice and humans with genetic deficiencies in interferon signaling are more susceptible to severe viral disease[11,12]. However, aberrant interferon expression can also promote harmful immunopathology[1,3,13]. Therefore, the probability and magnitude of interferon induction must exist within a narrow range to support host health.

The frequency of interferon induction early in infection is shaped by the molecular interactions between host and virus within infected cells. Interferon signaling is activated when cellular receptors bind pathogen-associated molecular patterns (PAMPs) from the virus, or damage-associated molecular patterns (DAMPs) from the host cell. In influenza infection, RIG-I is the host receptor responsible for activating interferon signaling in epithelial cells[14,15]. This process is antagonized by the flu protein NS1[16]. Flu populations lacking NS1 trigger an enhanced interferon response, which is dependent on *de novo* generation of viral RNA[17]. Influenza RNA is produced by two canonical mechanisms. First, incoming viral ribonucleoproteins (vRNPs) containing the negative-sense viral genome segments are transcribed in the nucleus to generate capped and polyadenylated mRNAs. After these mRNAs are translated to produce viral proteins, newly synthesized viral polymerases replicate the genomes, generating positive-sense complementary RNP (cRNP) intermediates and new negative-sense vRNPs[18]. The primary RIG-I ligand in influenza infection is thought to be the viral RNA genomes, which have a 5' triphosphate and a double-stranded region where the complementary 5' and 3' ends bind to each other[19]. Various aberrant viral RNAs have been shown to associate with enhanced interferon responses to influenza, including defective viral genomes (DVGs) and mini viral RNAs (mvRNAs)[20–24].

In addition to viral factors either positively or negatively influencing the interferon response, a number of different host pathways can impact its induction. Even when provided with a pure, uncomplicated, innate immune agonist such as the dsRNA mimetic poly(I:C), interferon is still produced in only a fraction of cells, implying that there may be layers of host regulation and stochasticity governing the probability of interferon production[7,8,25]. During infection, host processes may generate DAMPs, and interferon signaling triggers positive and negative cellular feedback loops that regulate further interferon production[26–30]. Other host factors influence viral progression through the life cycle, which is itself a highly heterogeneous process often varying in productivity by several orders of magnitude, and might therefore influence the probability of detection[31,32]. Therefore, the magnitude of the interferon response in a given viral infection is the result of a complex network of interacting factors that contribute in different contexts. Which host and viral processes influence the generation, propagation, and detection of immunostimulatory ligands in contexts relevant to human disease have not been clearly delineated.

Nonetheless, there have been very few studies comprehensively searching for host factors that modulate interferon induction[33,34]. One reason for this is the difficulty of performing a large-scale screen for genes that affect a probabilistic process. Because natural stimuli induce interferon in only a fraction of cells[4,6], a large number of cells would be required in order to achieve sufficient statistical power to detect effects of particular gene edits on the number of interferon-producing cells. As an alternative, other studies have used the expression of ISGs as a readout for interferon signaling because they are widely induced by exogenously added interferon[35–37]. However, here we focus on the initial interferon induction event. Additionally, we are interested in effects on the probability of induction as well as effects on the magnitude of interferon transcription in interferon-expressing cells, which is difficult to discern by binary selection. To address these challenges, we developed a novel CRISPR screening strategy that measures the effects of different gRNAs on transcription levels from a promoter of interest, which we have termed CRISPR with Transcriptional Readout (CRITR-seq).

Using our newly-developed method, we have performed a genome-wide screen for host factors that modulate interferon transcription in response to influenza A virus infection. We identified both canonical RIG-I signaling pathway members as well as host genes that interface with the viral life cycle. Among these, we found that loss of the Negative Elongation Factor (NELF) complex leads to increased flu transcription, which corresponds with a dramatic increase in interferon induction. These results have led us to more broadly identify viral transcription as a key contributor to interferon induction by flu.

Results

CRISPR with Transcriptional Readout (CRITR-seq) measures the effects of gRNAs on interferon transcription

CRISPR screens are a powerful tool to comprehensively search for novel interactions in biological processes. The most common form of CRISPR screen involves using CRISPR-Cas9 to generate a pool of edited cells, selecting for a phenotype of interest, and sequencing the DNA of the selected cells to identify guide RNAs (gRNAs) that are enriched or depleted by selection. However, not all phenotypes are amenable to selection, particularly those that do not directly determine cell survival. Various studies have overcome this limitation by using reporter constructs and cell sorting to apply selection to phenotypes of gene expression. While these methods have been informative, they often reduce complex regulatory differences to a binary (yes/no) readout. To provide a more quantitative readout of factors that modulate gene expression, we designed a new CRISPR screen that directly measures the effects of different gRNAs on transcription levels from a promoter of interest.

Our approach, which we call CRISPR with Transcriptional Readout ("CRITR-seq"), is a modification and combination of two prior CRISPR methods. The first is a prior method from yeast, called CRISPR interference with barcoded expression reporter sequencing (CiBER-seq)[38]. CiBER-seq uses a barcode embedded downstream of a reporter promoter. After sequencing is used to link a barcode to the appropriate guide, transcribed barcodes are used to measure guide impacts on transcription at the reporter promoter. While this method is useful in yeast, the lentiviral constructs generally used for human CRISPR screens can recombine[39], making it difficult to link a barcode to a guide. To overcome this limitation, we incorporated the entire gRNA expression construct downstream of our reporter promoter, such that the guide would be present within the reporter RNA. We took inspiration for this approach from CROP-seq, which uses a similar design to recover guide RNA sequences from single-cell RNA-seq[40]. Our design is explained in Figure 1A-B.

In this study, we applied the CRITR-seq method to perform a genome-wide CRISPR knockout screen for factors that modulate interferon induction in response to influenza A virus. For this purpose, we used the promoter for the type III interferon *IFNL1*. In A549 cells, a lung epithelial carcinoma cell line, expression of type I and type III interferons are highly correlated, and we have previously validated that our reporter promoter correlates well with the transcriptional response at the endogenous promoter in this cell line[9]. In each cell containing the CRITR-seq construct, the gRNA is transcribed both by RNA polymerase III, leading to Cas9-mediated gene editing, and, separately, by RNA polymerase II whenever the interferon promoter is active, generating a poly-adenylated mRNA containing the gRNA sequence (Figure 1A).

After generating a pool of edited cells using a genome-wide library of gRNAs, the abundance of each gRNA sequence in the bulk mRNA should correlate with interferon transcription levels in cells containing that gRNA (Figure 1B). To account for the frequency of lentiviral integration for each gRNA, we normalized the read count of each guide in the mRNA to the corresponding number of reads in the genomic DNA (gDNA). We used Model-based Analysis of Genome-wide CRISPR/Cas9 Knockout (MAGeCK)[41] to calculate a statistical score for the enrichment or depletion of gRNAs targeting each gene, based on a null distribution drawn from the non-targeting guides. We expect that gRNAs targeting positive regulators of interferon expression will be depleted in the mRNA, while gRNAs targeting negative regulators will be enriched.

Interferon is produced by only a fraction of cells and is expressed at low levels, making it difficult to study in a selection-based screen. However, performing a CRISPR screen with transcription as the readout provides more sensitivity and allows us to identify factors that modulate either the probability or the magnitude of interferon induction in a flu infection. We expect that these factors include both direct regulators of the RIG-I signaling pathway, as well as host factors that interface with the viral life cycle to influence the generation or protection of immunostimulatory ligands.

Genome-wide CRITR-seq screen identifies factors required for RIG-I signaling or infection as positive regulators of the interferon response to influenza A virus

The workflow for the CRITR-seq screen in this study is shown in Figure 1C. We generated 3 independent CRITR-seq libraries by cloning gRNA sequences from the Genome-Scale CRISPR Knock-Out (GeCKO) library[42] into the CRITR-seq vector with the interferon promoter. This library targets 19,050 genes with 6 gRNAs per gene and includes 1000 different non-targeting gRNAs. We used these libraries to generate populations of edited cells in a clonal A549 line that constitutively expresses Cas9. Amplicon sequencing validated that the plasmid CRITR-seq libraries retained over 95% coverage of the GeCKO library guides; most of these guides were still maintained in the genomic DNA of the Cas9-edited cells (Figure S1). Loss in representation in the gDNA is likely due to a combination of stochastic dropout as well as the loss of gRNAs that target essential genes.

We infected the edited cell populations with a variant of influenza A virus which contains stop codons early in the NS1 open reading frame ($NS1_{mut}$, File S2). Genome segments 1-7 are from A/WSN/1933 (WSN) IAV, while segment 8 (encoding NS2 and the nonsense-mutated NS1) is from the A/Puerto Rico 8/1934 (PR8) genetic background, as we found including this segment from the PR8 strain increased viral titers. $NS1_{mut}$ lacks a functional NS1, while all other genes including NS2 remain intact. In the absence of NS1, IAV induces interferon in $\sim$20% of cells[9], raising the basal level of interferon induction to more easily detect modulations due to gene edits. We harvested cellular RNA and genomic DNA after 8 hours of infection. This early time point was chosen to capture the initial innate immune detection and to minimize potential confounding effects of paracrine signaling and multiple rounds of viral infection.

Amplicon sequencing and MAGeCK analysis revealed that a large fraction of the gRNA sequences were depleted in the mRNA (Figure 2A). This is likely a combination of biological signal (gRNAs targeting genes essential for the interferon response) and noise (stochastic dropout exacerbaed by the low probability of interferon induction in infected cells) (Figure S2). The issue of stochastic dropout in large-scale screens presents a statistical challenge for identifying biologically-relevant depleted gRNAs[41,46]. Thus, rather than following up individually with top-ranked hits, we instead assessed the effectiveness of the screen by looking to see where genes expected to be required for interferon induction fell in the mRNA/gDNA distribution. Validating our method, we see that gRNAs targeting most of the known members of the RIG-I signaling pathway[47–52] were depleted in the screen (Figure 2B, C). *IRF3*, the transcription factor immediately upstream of *IFNL1*, was the top-ranked hit for depleted genes.

In addition to having an intact RIG-I signaling pathway, cells need to be infected to produce interferon. Thus,

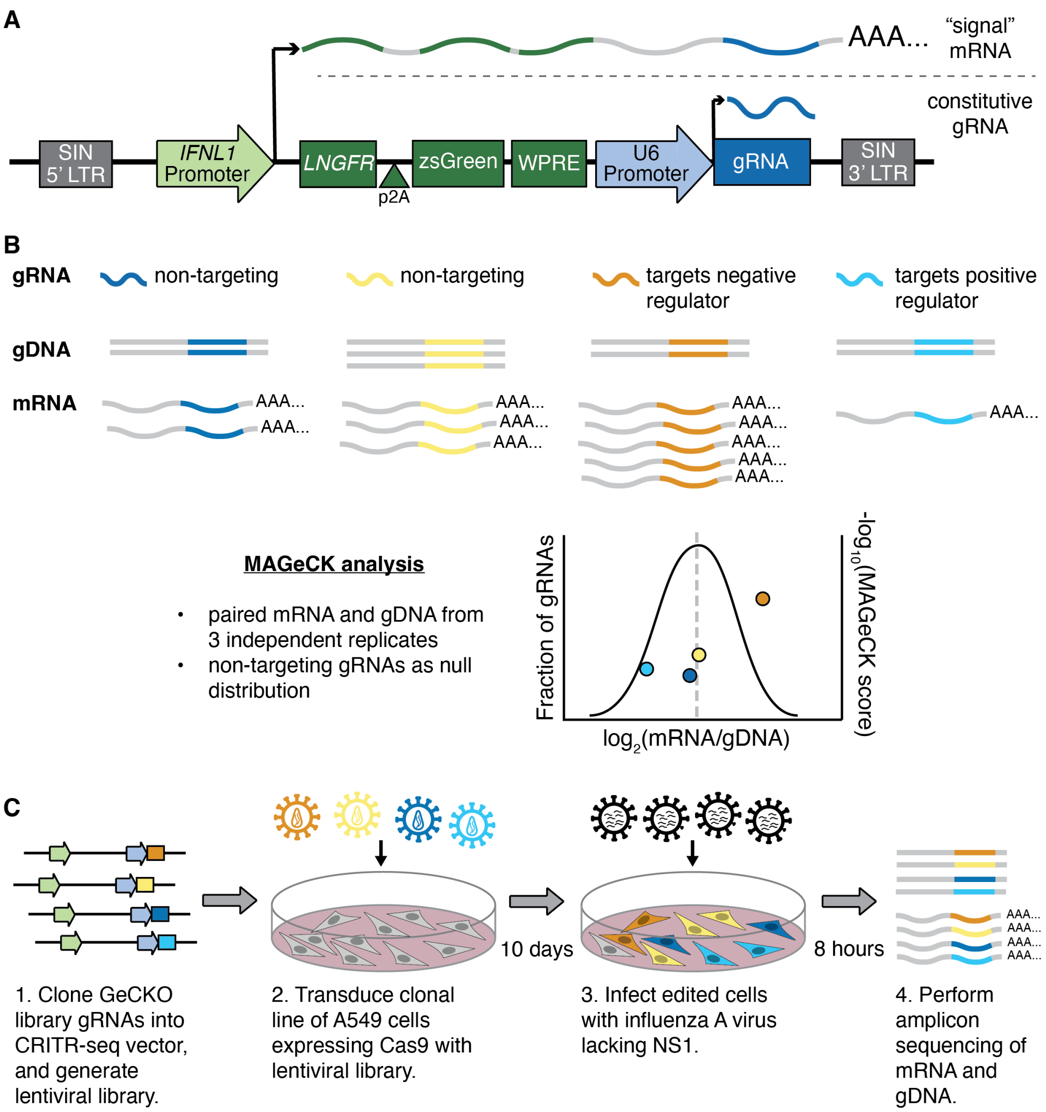

Figure 1. CRISPR with Transcriptional Readout (CRITR-seq) measures the effects of gRNAs on interferon transcription

(A) CRITR-seq vector with a type III interferon reporter. Functional gRNA is constitutively transcribed from the U6 promoter. gRNA sequence is also present in the reporter mRNA transcribed from the *IFNL1* promoter, serving as a barcode indicating which edit occured in the transcribing cell. SIN LTR = self-inactivating long terminal repeat, *LNGFR* = low-affinity nerve growth factor receptor, WPRE = woodchuck hepatitis virus posttranscriptional regulatory element.

(B) Model of amplicon sequencing and data analysis of CRITR-seq screen. Amplicon sequencing is performed on the gRNA-containing regions of the genomic DNA and polyadenylated mRNA. The mRNA/gDNA ratio for each gRNA sequence represents the normalized *IFNL1* transcription levels for that guide. Graph represents a distribution of all gRNAs based on their mRNA/gDNA ratio, with individual examples highlighted as colored points plotted based on their hypothetical Model-based Analysis of Genome-wide CRISPR/Cas9 Knockout (MAGeCK)[41] score.

(C) Workflow for the CRITR-seq screen in this study. 3 libraries were generated independently, starting from PCR-amplifying the gRNAs out of the GeCKO library[42]. A clonal line of Cas9-expressing A549 cells was transduced with lentivirus carrying the CRITR-seq vector at an MOI of 1.5, with an assumption that most gRNAs would not affect the interferon induction phenotype, so very little epsitasis would complicate our measurements. After allotting 10 days for gene editing, edited cells were infected with $NS1_{mut}$ influenza A virus at an MOI of 2 based on qPCR titer.

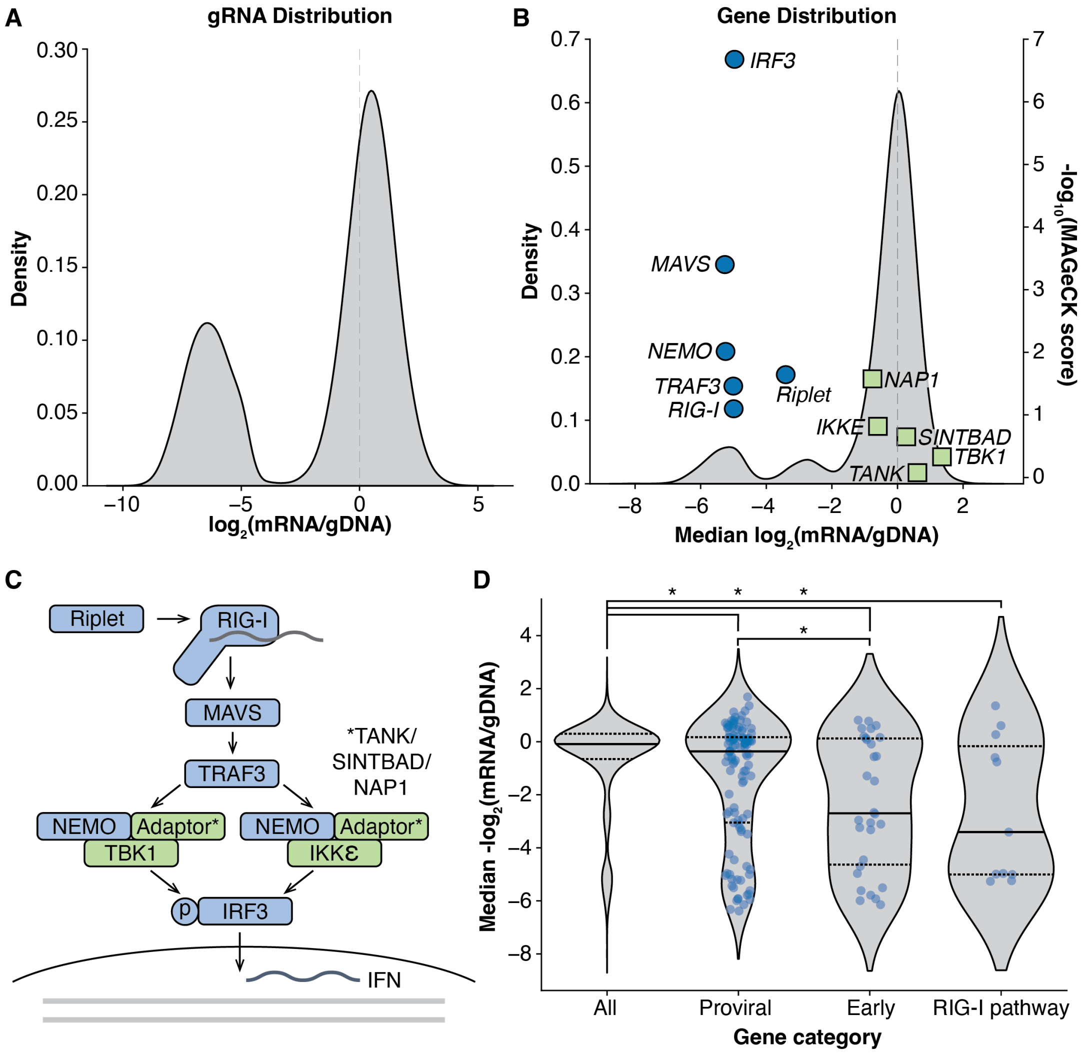

Figure 2. Genome-wide CRITR-seq screen identifies factors required for RIG-I signaling or infection as positive regulators of the interferon response to influenza A virus

(A) Distribution of gRNAs across all 3 replicates of the CRITR-seq screen, based on mRNA/gDNA ratio. gRNAs with less than 25 reads in genomic DNA in any replicate were excluded from analysis. Read counts across replicates were normalized based on the non-targeting gRNAs from each replicate.

(B) Distribution of genes based on the median mRNA/gDNA ratio for surviving guides targeting that gene across all 3 replicates. Individual genes from the RIG-I signaling pathway, shown in (C), are plotted based on their MAGeCK robust ranking aggregation score for depletion in the mRNA. MAGeCK statistical scores were calculated using non-targeting gRNAs as the null distribution, with depletion in the mRNA as the alternative hypothesis.

(C) RIG-I signaling pathway. Genes/proteins in blue are considered essential for interferon induction through this pathway, while genes/proteins in green may be partially redundant. *IRF7* was excluded from this analysis because in epithelial cells it is expressed at very low levels prior to interferon signaling and likely does not contribute to interferon transcription at this early time point[43,44].

(D) mRNA/gDNA ratios from (B), subsetted by gene category. "Proviral" genes were identified by Li et al.[45] in a CRISPR screen for genes required for influenza infection in A549 cells. "Early" genes are a subset of the proviral genes annotated to be involved in viral entry, nuclear import, viral transcription/replication, or nuclear export. Proviral and Early genes tested are listed in Table S1. RIG-I pathway genes are those shown in (C). Solid lines represent the median; dotted lines represent the first and third quartiles. * indicates ANOVA $p<0.05$, post-hoc Tukey's test $q<0.05$.

we also explored genes identified in a previous screen that are required for flu infection (Table S1)[45]. As with the members of the RIG-I pathway, the proviral factors tended to be depleted in the mRNA (Figure 2D). This depletion was even more pronounced for the subset of proviral genes involved in early steps of the viral life cycle (viral entry, nuclear import, transcription/replication, and nuclear export) which may precede or contribute to the production of innate immune ligands.

Loss of the Negative Elongation Factor complex enhances interferon induction by flu

We next examined the genes with guides enriched in the mRNA. Strikingly, the top three enriched genes in our screen were all components of the Negative Elongation Factor (NELF) complex: *NELFB*, *NELFA*, and *NELFCD* (Figure 3A). The NELF complex — made up of NELF-A, NELF-B, either NELF-C or NELF-D, and NELF-E — is conserved in many metazoans from *Drosophila* to humans. During transcription, it transiently associates with RNA polymerase II, mediating a promoter-proximal pause ∼20-60 nucleotides downstream of the transcription start site[53–57]. This acts as a checkpoint between transcription initiation and elongation, regulating the kinetics of transcription for most human mRNAs[58–61]. The pause before productive elongation is also the stage at which capping enzymes add an m^7G-cap to the 5' end of the nascent mRNA, which is important for mRNA stability, export from the nucleus, and translation[62–64]. In the absence of NELF, RNA polymerase II does not pause at the promoter-proximal region, but instead stalls further downstream, near the location of the +1 nucleosome[60,65].

The NELF complex has not previously been identified as regulating the transcription of interferons, nor has it been associated with influenza growth and replication. To ensure that our results from the screen were not specific to the reporter construct, but were consistent with effects at the endogenous interferon loci, we sought to validate our findings with single knockouts. Using single CRISPR guides with ribonucleoprotein transfection, we knocked out *NELFA*, *NELFB*, and *NELFCD* and measured type I and III interferon transcription during infection with $\mathrm{NS1}_{\mathrm{mut}}$. We did not establish clonal lines for these experiments as NELF is essential for cell proliferation[65]. Each gene we tested matched our predictions from CRITR-seq, with over a 30-fold increase in interferon transcription upon loss of *NELFB* (Figure 3B). The same effects were observed for type I interferon transcription, demonstrating that any impacts of NELF cannot be limited to the *IFNL1* locus and likely globally impact interferon production during flu infection.

As we validated our three NELF targets identified through a genome-wide screen, we chose to focus on one, *NELFB*, for further characterization. Prior experiments have demonstrated co-dependence of NELF components, so depletion of a single member of this complex should be sufficient to impair its function[65,66]. Because it is possible for CRISPR edits, which generally knockout a gene, to generate truncated proteins that may act as hypo- or hypermorphs in a complex, we decided to use siRNA-mediated knockdown of *NELFB* for further experiments to simplify interpretations. Consistent with the CRISPR-Cas9 results, knockdown of *NELFB* increased interferon transcription in response to both $\mathrm{NS1}_{\mathrm{mut}}$ and wildtype WSN influenza (Figure 3C-D, S3, S4). Thus, depletion of NELF increases interferon induction even in the presence of NS1.

To determine if the effects of *NELFB* knockdown were flu-specific, we examined its effects both in the absence of infection and when cells were challenged with a dsRNA mimetic, poly(I:C). In both cases, no changes in interferon transcription were observed (Figure 3E-F). This means that the impacts we observe are unlikely to be due to universal upregulation of transcription at the interferon loci, or to general cellular perturbation generating innate immune ligands independent of infection.

Loss of NELF increases canonical flu transcription

Given than NELF depletion does not affect the interferon response to poly(I:C), we wondered whether it may act upstream of RIG-I activation by influencing some stage of the viral life cycle. We tested whether loss of NELF impacts flu RNA levels in the cell. Indeed, we found that for both $\mathrm{NS1}_{\mathrm{mut}}$ and wildtype virus, knockdown of *NELFB* led to an increase in RNA encoding the viral gene *HA*, as measured by qPCR that detects all types of viral RNAs (Figure 4A). To narrow down the step at which the NELF complex modulates viral RNA production, we tested the effect of NELF depletion on an influenza variant incapabale of genome replication, $\mathrm{PB1}_{455:350}$[67]. This virus contains a large internal deletion in the gene segment encoding the polymerase subunit PB1. As a result, it can engage in primary transcription of the incoming vRNPs but cannot produce the functional polymerase required to generate cRNPs and vRNPs. In $\mathrm{PB1}_{455:350}$ infection, *NELFB* knockdown increased *HA* RNA levels (Figure 4B), demonstrating that the increased RNA does not depend on viral replication.

These results suggest NELF may be interacting with flu transcription. Influenza transcription initiation requires

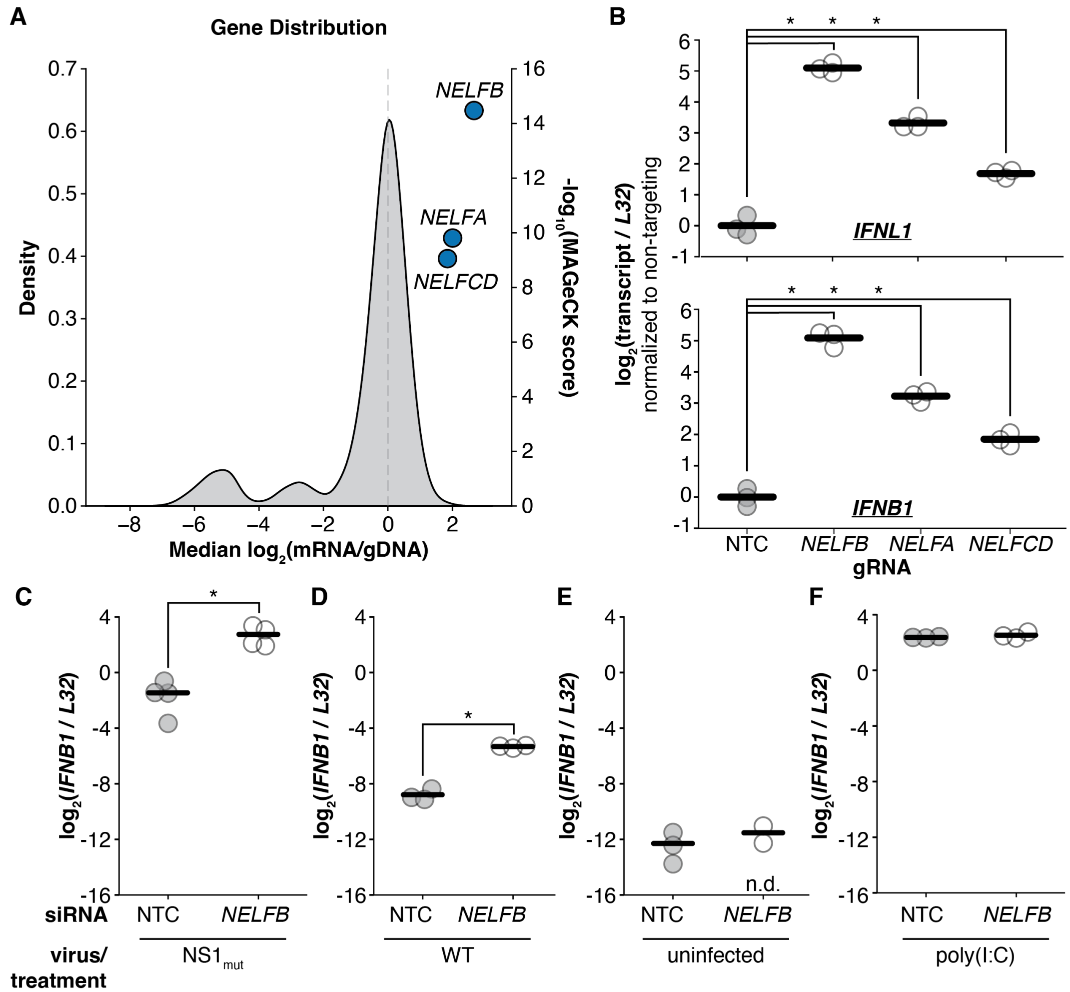

Figure 3. Loss of the Negative Elongation Factor complex enhances interferon induction by flu
(A) Same distribution of genes from CRITR-seq screen as in Figure 2B, but with the top 3-ranked genes enriched in the mRNA highlighted. MAGeCK statistical scores here were calculated with enrichment in the mRNA as the alternative hypothesis, using non-targeting gRNAs as null distribution.
(B) A549 cells were transfected with Cas9-gRNA ribonucleoprotein complexes with gRNAs targeting the indicated genes. After passaging 10 days to allow for gene editing, cells were infected with $NS1_{mut}$ at a genome-corrected MOI of 2. RNA was harvested at 8 hours post-infection for qPCR analysis of *IFNB1* and *IFNL1* transcripts. NTC = non-targeting control.
(C-D) A549 cells were treated with siRNA for 9 days and then infected with $NS1_{mut}$ at a genome-corrected MOI of 1 (C) or WT WSN at an infectious MOI of 1 (D). RNA was harvested 8 hours post-infection for qPCR analysis. The same results were obtained for the WSN $NS1_{stop}$ virus (with WSN genetic background for all segments), shown in Figure S4. Validation of *NELFB* knockdown is shown in Figure S3.
(E) A549 cells were treated with siRNA for 9 days before harvesting RNA for qPCR. n.d. = not detected. Validation of *NELFB* knockdown is shown in Figure S3.
(F) A549 cells were treated with siRNA for 9 days and transfected with 50 ng poly(I:C) for 8 hours before harvesting RNA for qPCR. Validation of *NELFB* knockdown is shown in Figure S3.
Biological replicates are shown as individual data points, with lines representing the means. One-tailed t-test (B) with increased expression as the alternative hypothesis, or two-tailed t-tests (C-F) were performed to compare each treatment with the non-targeting control. n=3 (B,D-F) or n=4 (C). * indicates $p<0.05$ after Benjamini-Hochberg multiple hypothesis correction.

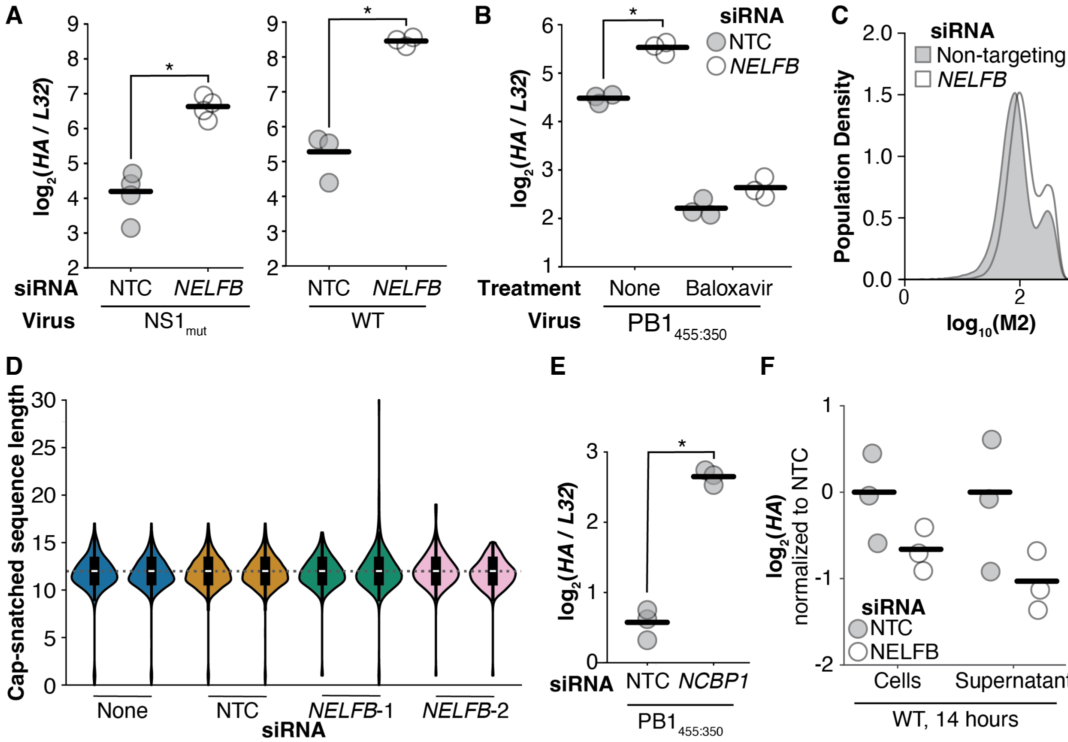

Figure 4. Loss of NELF increases canonical flu transcription

(A) RNA from experiment performed in Figures 3C and 3D, with *HA* transcripts measured by qPCR. The same results were obtained for the WSN $NS1_{stop}$ virus, shown in Figure S4. NTC = non-targeting control.

(B) A549 cells were treated with siRNA for 9 days. Cells were infected with $PB1_{455:350}$ at an infectious MOI of 1, with or without 100 nM baloxavir acid added at time of infection. RNA was harvested 8 hours post infection for analysis by qPCR. Validation of *NELFB* knockdown is shown in Figure S3.

(C) An A549 *IFNL1* reporter cell line was treated with siRNA for 9 days and infected with $NS1_{mut}$ at a genome-corrected MOI of 1. 13 hours post infection, cells were stained for the viral protein M2 and fixed for flow cytometry. Graph shows distribution of M2 staining normalized for unit area, for one representative replicate. Full flow data shown in Figure S5.

(D) A549 cells were treated with either of 2 different *NELFB*-targeting siRNAs, a non-targeting control, or no siRNA, with 2 biological replicates per treatment. After 9 days of siRNA treatment, cells were infected with $NS1_{mut}$ at a genome-corrected MOI of 2. RNA was harvested 8 hours post infection, and 5' RACE was performed on polyadenylated mRNAs, followed by sequencing. Cap-snatched sequence length refers to the number of nucleotides between the template switch oligo sequence and the +1 position of the flu mRNA sequence. Violin plots contain box plots for each sample, and the median of all samples is represented by the gray dotted line. Violin plot whiskers extend to the most extreme points in the dataset, excluding the top 2% of lengths. Validation of *NELFB* knockdown phenotype is shown in Figure S6.

(E) A549 cells were treated with siRNA for 4 days and infected with $PB1_{455:350}$ at an infectious MOI of 1. RNA was harvested 8 hours post infection for analysis by qPCR.

(F) A549 cells were treated with siRNA 9 days before infection with WT WSN at an infectous MOI of 5. Media was replaced with fresh IGM 2 hours post infection. 14 hours post infection, viral supernatant was collected and cells were lysed for RNA extraction. Reverse transcription was performed using universal influenza primers for the RNA from the supernatant, and random hexamer primers for the RNA from the cell lysate. Further qPCR analysis is shown in Figure S7.

For panels A-B and E-F, biological replicates are shown as individual data points, with lines representing the means. Two-tailed t-tests were performed to compare targeted siRNA with the non-targeting control. n=4 (A, left) or n=3 (A, right; B; E-F). Benjamini-Hochberg multiple hypothesis correction was performed for panels B and F. * indicates $p<0.05$.

the viral polymerase to bind actively-transcribing host RNA polymerase II and a nascent, capped host mRNA[68–71]. The flu polymerase then "snatches" the cap and 5' terminus of the host transcript, which becomes the primer for flu transcription[72,73]. This interaction is thought to occur during the promoter-proximal pause of RNA polymerase II[68,74,75], which is the stage stabilized by binding of NELF. Given that NELF depletion affects RNA polymerase II pausing dynamics[60,65,76], we hypothesized that loss of NELF also affects flu cap-snatching and transcription in an infected cell.

To test this hypothesis, we treated cells with baloxavir, a drug that blocks cap-snatching by inhibiting the endonuclease activity of the flu polymerase subunit PA[77]. The effect of *NELFB* knockdown on *HA* RNA levels was mostly suppressed by baloxavir treatment (Figure 4B, S3), so we conclude that the increased flu RNA upon NELF depletion is due to increased flu transcription. The slight residual increase in *HA* RNA upon *NELFB* knockdown for the baloxavir-treated infections may be due to either incomplete inhibition of cap-snatching by baloxavir, or the generation of RNA through an additional mechanism independent of canonical transcription.

To determine whether flu RNAs generated in the absence of NELF were canonical viral mRNAs, we first used flow cytometry to determine whether the increased flu RNA is accompanied by increased abundance of viral proteins. Indeed, knockdown of *NELFB* led to higher levels of the flu protein M2 (Figure 4C, S5), indicating that NELF depletion increases productive flu transcription. Next, we tested whether loss of NELF impacts the length of the cap-snatched host mRNA fragments. We performed 5' Rapid Amplification of cDNA Ends (RACE) on RNA extracted from flu infections in cells treated with either non-targeting control or *NELFB*-targeting siRNA. After aligning the 5' mRNA sequences with flu mRNA sequences, we considered the snatched host mRNA sequence to be all bases upstream of the +1 position of the viral mRNA sequence. *NELFB* knockdown does not seem to affect the distribution of cap-snatched sequence lengths (Figure 4D, S6). In both the presence and absence of *NELFB*-targeting siRNA, the cap-snatched host sequences matched the expected lengths of 8-14 nucleotides shown in previous studies[72,78], with a median length of 12 nucleotides. Taken together, these results suggest that canonical, productive flu transcription increases when NELF is depleted.

We further wanted to explore the host-virus interface that impacts the rate of flu transcription. Shortly after 5' caps are added to nascent mRNA, these caps are bound by the cap-binding complex (CBC), a heterodimer of nuclear cap binding protein (NCBP) 1 and 2, which could, in theory, compete with flu polymerase for binding to host mRNA cap structures[79,80]. NELF has been shown to associate with the cap-binding complex, and NELF depletion leads to a general decrease in NCBP1 occupancy on chromatin[64–66,81]. Therefore, we hypothesized that flu transcription increases in the absence of NELF due to increased availability of capped nascent mRNAs not bound by CBC. To determine the impact of CBC presence on flu transcription, we treated cells with siRNA targeting *NCBP1* and then infected them with $PB1_{455:350}$. *NCBP1* knockdown led to increased levels of *HA* RNA for this primary transcription-only virus (Figure 4E), demonstrating that decreased levels of the cap-binding complex increase influenza transcription. These data are consistent with a model that NELF depletion increases influenza transcription via decreased recruitment of CBC (Figure 7), although we could not verify this mechanism through NELF/CBC epistasis experiments due to the loss of fitness incurred from both interventions.

Finally, we wanted to explore how increased transcription upon NELF depletion affects the flu life cycle overall. We measured viral RNA levels in both cells and supernatant 14 hours post infection by wild-type virus. This time point should allow us to observe any net effect on production of viral progeny, with minimal influence from autocrine and paracrine interferon signaling. We found that after 14 hours of infection, total flu RNA levels in the cell are unaffected by *NELFB* knockdown (Figure 4F, S7). Given previous findings that flu transcripts can make up over half the total cellular transcriptome later in infection[31], it would make sense that flu transcription is initially accelerated upon NELF depletion but is perhaps eventually limited by other factors, reaching the same saturation point as in the presence of NELF. Knockdown of *NELFB* also did not increase viral titer in the supernatant, as measured by qPCR, showing that the increased transcription early in infection is not sufficient to increase production of viral progeny.

Loss of NELF increases the generation of RIG-I ligands by flu

When NELF is depleted, the increased levels of viral transcription likely lead to a subsequent increase in viral replication due to the more rapid accumulation of viral proteins required for genome replication. Our observation that *NELFB* knockdown increases viral *HA* levels ∼2-fold for a replication-incompetent virus but ∼10-fold for wild-type flu (Figure 4B; 4A, right) further suggests that NELF depletion increases the generation of both flu transcripts and, as a consequence, genomic vRNA. With this synergistic increase in flu RNAs, we hypothesized that the large increase in intereron induction when NELF is depleted is due to increased production of immunostimulatory ligands.

To determine whether viral RNAs generated through transcription and replication are responsible for the en-

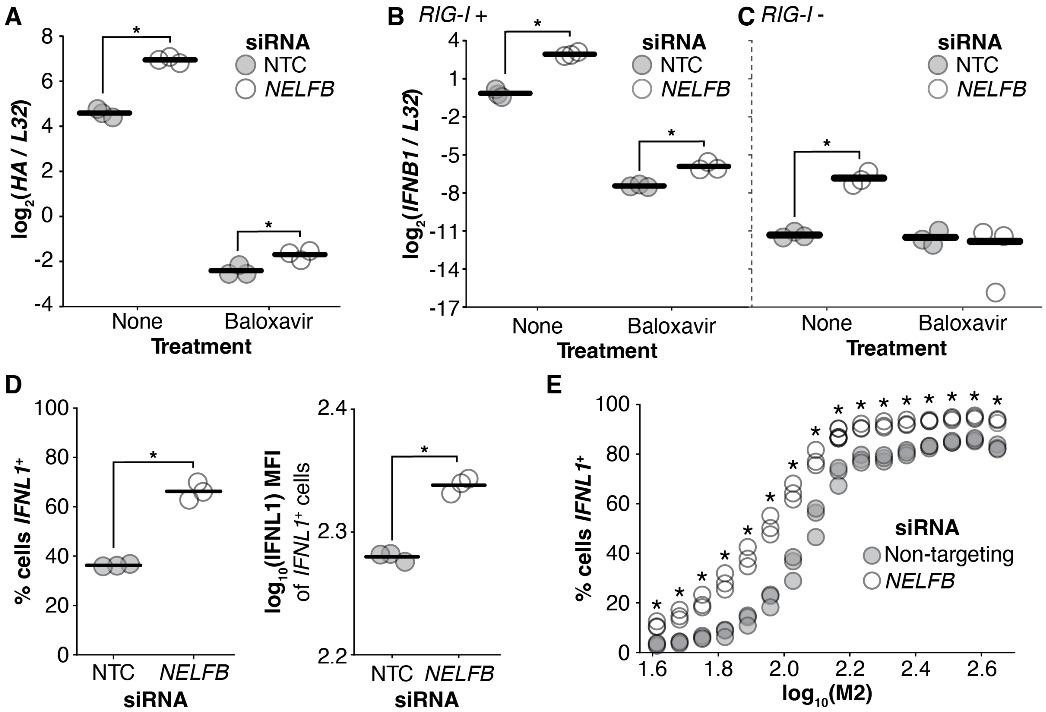

Figure 5. Loss of NELF increases the generation of RIG-I ligands by flu
(A-C) Wild-type A549 cells (A-B) or a *RIG-I*-knockout cell line derived from a single cell clone (C) were treated with siRNA for 9 days. Cells were infected with $NS1_{mut}$ at a genome-corrected MOI of 1, with or without 100 nM baloxavir acid added at time of infection. RNA was harvested 8 hours post infection for qPCR analysis. NTC = non-targeting control. We note the *RIG-I*-knockout cell line has some residual RIG-I expression observed by Western blot after flu infection (Figure S8). *HA* qPCR measurements in these cells are shown in Figure S9.
(D) Flow cytometry experiment from Figure 4C, with zsGreen *IFNL1* reporter results shown. Left: %*IFNL1*$^+$ cells determined as the percent of cells positive for zsGreen expression. Right: mean fluorescence intensity (MFI) of zsGreen for *IFNL1*$^+$ cells. Full flow data shown in Figure S5.
(E) Cells from (D) were divided into bins based on levels of M2 staining. %*IFNL1*$^+$ cells plotted for each bin. Bins with less than 100 events were removed from plotting and analysis.
Points represent biological replicates, with lines indicating the means. Two-tailed t-tests were performed comparing the *NELFB* siRNA samples with the non-targeting control for each treatment condition (A-D) or for each M2 expression bin (E), n=3. * indicates $p<0.05$ after Benjamini-Hochberg multiple hypothesis correction.

hanced interferon induction upon loss of NELF, we knocked down *NELFB* and infected cells with $NS1_{mut}$ influenza in the presence or absence of baloxavir. Baloxavir treatment ablated 99.9% of the increase in *HA* RNA upon *NELFB* knockdown (Figure 5A, S3). Therefore, the vast majority of the increased RNA upon NELF depletion can be attributed to the process of viral transcription — either directly, or indirectly through its support of genome replication. In this experiment, the baloxavir treatment also suppressed 99.8% of the increase in interferon induction caused by *NELFB* knockdown (Figure 5B), suggesting that enhanced interferon caused by loss of NELF is largely dependent on *de novo* viral RNA generated through transcription and/or replication.

We repeated this experiment in a *RIG-I*-knockout A549 cell line generated in our lab (Figure S8). In these cells, *NELFB* knockdown led to only 0.12% of the increase in interferon expression compared to wild-type cells (Figure 5C, S3, S9). This increase could be due to residual RIG-I present in these knockout cells or caused by alternate cellular interferon induction pathways (e.g., through MDA5 or cGAS/STING). However, the vast majority of enhanced interferon induction upon NELF depletion was RIG-I-dependent, which is the pathway we would anticipate to be triggered by increased flu RNA.

We expect that increased concentration of immunostimulatory ligands increases the probability of productive receptor-ligand interactions, leading to earlier and more frequent activation of the interferon induction pathway. Consistent with this model, flow cytometry performed on infected cells with an *IFNL1* zsGreen reporter showed that

NELFB knockdown led to both a greater fraction of interferon-expressing cells and increased interferon expression per cell (Figure 5D).

Is this effect merely an acceleration of the canonical flu life cycle? Or is removal of NELF not simply enhancing flu transcription, but also, concurrently, increasing the production of some aberrant immunostimulatory product? In support of the latter hypothesis, we find that if we divide infected cells into bins based on their level of M2 staining, *NELFB* knockdown leads to a higher frequency of interferon induction at each level of M2 expression (Figure 5E). This indicates that the increased interferon expression is higher than expected if solely based on increased productive transcription, suggesting there may be additional aberrant RNAs generated upon NELF depletion that also contribute to interferon induction.

Influenza transcription contributes to interferon induction even in the absence of viral genome replication

We have seen that upon NELF depletion, the majority of the enhanced interferon induction by $NS1_{mut}$ influenza can be attributed to increased viral transcription. Since multiple types of viral RNAs, including both transcripts and genomes, are increased in this context, we wanted to determine whether transcription itself participates in interferon induction, apart from its role in promoting genome replication. Here we are interested in exploring ligands that contribute to the interferon response in human infections, so we focused on the more biologically-relevant context: infection in the presence of NELF. To determine the specific role of transcription in interferon induction, we infected wild-type A549 cells in various conditions that do not permit viral replication. Critically, by standard models of RIG-I behavior and viral transcription, this is not a step that should be associated with the induction of an interferon response.

First, we infected cells with $PB1_{455:350}$ and treated them with drugs that specifically inhibit influenza transcription via two different mechanisms: baloxavir, which inhibits the cap-snatching endonuclease activity of the polymerase subunit PA[77], or pimodivir, which blocks the ability of the polymerase subunit PB2 to bind to host mRNA caps[82]. For this replication-incompetent virus, both baloxavir and pimodivir inhibited viral RNA generation (Figure 6A), confirming they effectively inhibit flu transcription. Surprisingly, they also both suppressed interferon induction to a large degree, although not quite to uninfected levels (Figure 6B). Therefore, interferon induction by this defective virus is significantly dependent on transcription.

It is possible that $PB1_{455:350}$, a virus with a particular defective genome, may have unique immunostimulatory features that do not generally drive interferon induction in other flu populations. We then tested a nominally wild-type population, characterized previously[17], that contains a high burden of defective viral particles to maximize the observed interferon response. Because this population contains replication-competent viruses, we treated cells with cycloheximide upon infection to inhibit protein translation and thus prevent viral replication. In the presence of cycloheximide, baloxavir treatment decreased interferon levels by this heterogeneous viral population (Figure 6C-D). We interpret these results with the caveat that cycloheximide itself increases interferon induction to different stimuli, including poly(I:C)[83]; the particular ligand enhanced by cycloheximide treatment is unknown and may not correspond to the primary ligand in a typical flu infection. However, the finding that baloxavir treatment reduces interferon expression in this context is an additional demonstration that flu transcription can contribute to interferon induction even in the absence of viral replication.

Discussion

Here we report the first transcription-based genome-wide CRISPR screen for genes that influence interferon induction. To accomplish this goal, we developed CRISPR with Transcriptional Readout, or CRITR-seq, in which each gRNA sequence serves as a barcode in a longer mRNA, associating the edit with transcription at a reporter promoter (in this study a type III interferon promoter).

In applying CRITR-seq to identify host factors that modulate interferon induction by flu, we observed that many of the genes with the strongest effect sizes, both positive and negative, directly affect the flu life cycle. Gene edits that ablate interferon induction included not only members of the RIG-I signaling pathway, but also viral dependency factors required for host cell entry and the generation and nuclear export of *de novo* viral RNAs. Similarly, the top three hits for gene edits with enhanced interferon induction were all members of the NELF complex, which we have now defined as influencing viral transcription. These results suggest that some of the strongest observable host effects on interferon induction come from factors that impact the flu life cycle. This finding is consistent with our

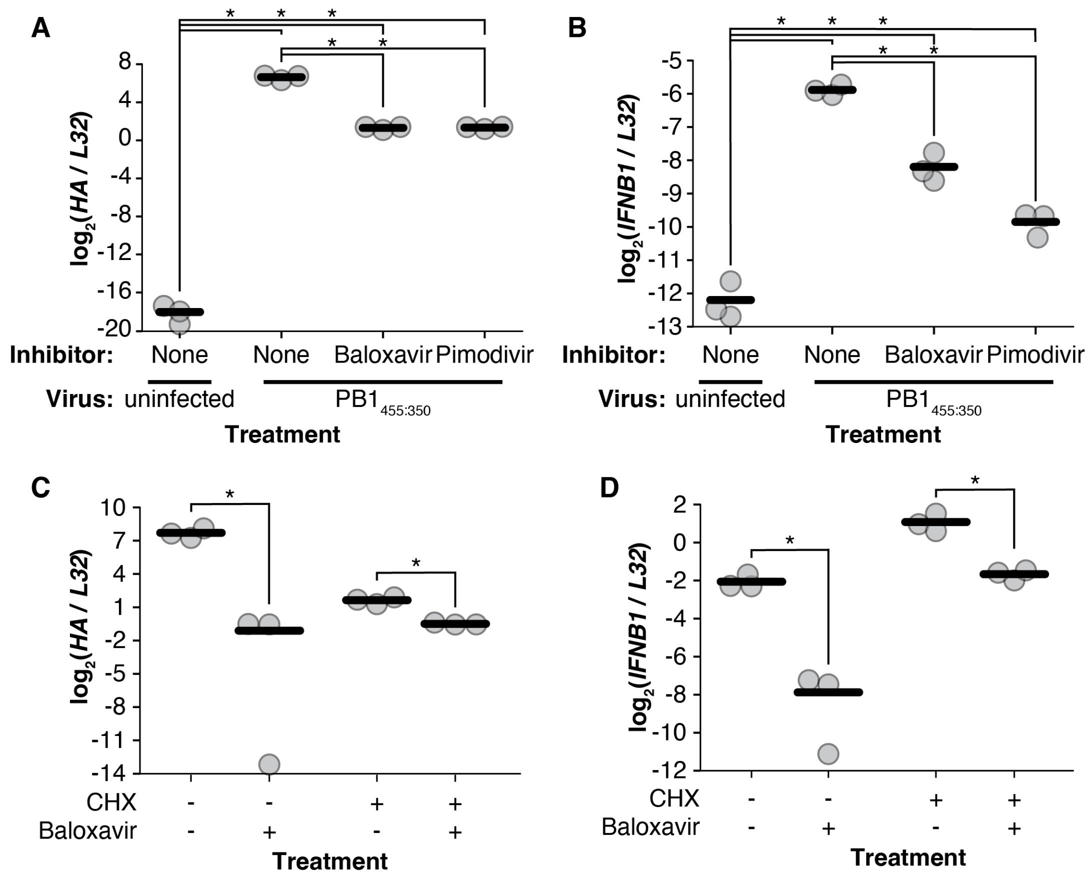

Figure 6. Influenza transcription contributes to interferon induction even in the absence of viral genome replication

(A-B) A549 cells were infected, or not, with $PB1_{455:350}$, at an infectious MOI of 1, with or without 100 nM baloxavir acid or 100 nM pimodivir added 2 hours prior to infection. RNA was harvested 14 hours post infection for qPCR analysis.

(C-D) A549 cells were infected with a high-defective population of WT WSN at an MOI of 2 based on qPCR titer. For drug treatments, cells were treated with 10 nM baloxavir acid and/or 50 μg/mL cycloheximide (CHX) at time of infection. RNA was harvested 9 hours post infection for qPCR analysis.

Points represent biological replicates, with lines indicating the means. For A and B, two-tailed t-tests were performed comparing each treatment with the uninfected sample and with the infected sample without inhibitors, n=3. For C and D, two-tailed t-tests were performed comparing presence and absence of baloxavir, for each CHX condition, n=3. * indicates $p<0.05$ after Benjamini-Hochberg multiple hypothesis correction.

previous work which showed that in the absence of NS1, higher levels of interferon induction were associated with higher levels of flu RNA[17]. Taken together, we propose that the concentration of immunostimulatory ligands, which is modulated by both host and viral factors, is one of the primary drivers of the probability of interferon induction during influenza infection.

Our top hit, the NELF complex, has not previously been defined as a key host interface for influenza A virus. NELF depletion led to a massive increase in interferon induction at an early infection time point, which we found to be largely due to an increase in flu transcription and thus enhanced generation of immunostimulatory ligands. These findings reveal new roles for the host transcription machinery in modulating ordered progression through the flu life cycle. Loss of NELF accelerates transcription early in infection but does not increase the total flu RNA levels or production of progeny that the virus eventually achieves. It seems that enhancement at this early step of RNA generation does not benefit the virus but instead increases opportunity for detection by cell intrinsic innate immunity, thereby disrupting mechanisms controlling progression through the viral life cycle that seem to minimize this detection.

It is surprising that NELF depletion increases viral RNA production even for a replication-incompetent virus, as

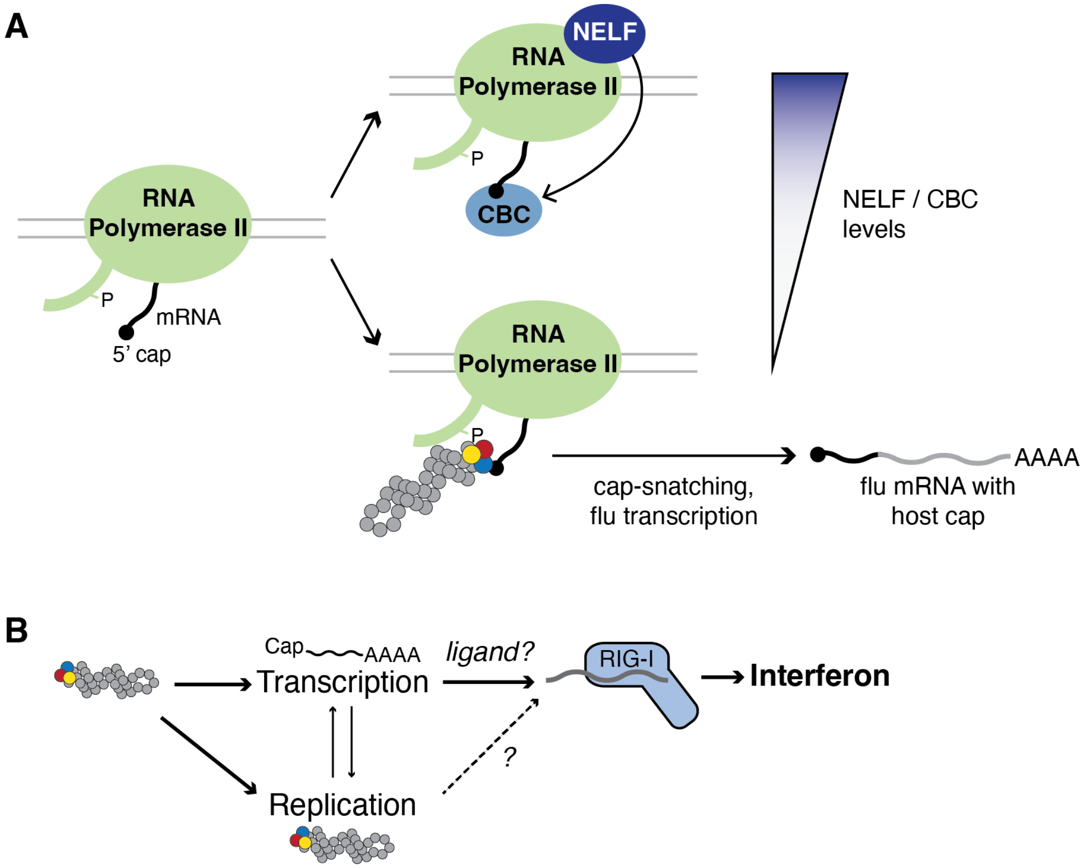

Figure 7. Summary of findings from this study
(A) Influenza polymerase binds preferentially to RNA polymerase II with serine 5 phosphorylation in the C-terminal domain (CTD), which is the state that is characteristic of the promoter-proximal pause[64,68]. In our proposed mechanism, flu polymerase and cap-binding complex (CBC) compete for binding to nascent host mRNA caps. This is consistent with the finding in this study that depletion of NELF, which decreases CBC binding, increases flu cap-snatching and transcription.
(B) Contributions of *de novo* viral RNA generation to interferon induction. Flu transcription, both in the presence and absence of viral replication, contributes to interferon induction. The transcription-dependent immunostimulatory ligand(s) remain unknown. Flu replication also contributes to interferon induction, which may occur through its support of the transcription-dependent ligand, or additionally through replication products (i.e., viral genomes).

under these circumstances there are only 8 individual RNA molecules undergoing transcription at a given time. This suggests that establishing a productive interaction between the flu polymerase and the nascent capped host mRNAs is a rate-limiting process for viral RNA generation even when flu polymerase concentrations are incredibly low. We do not know exactly how the presence of the NELF complex limits the rate at which this interaction occurs. Given that knockdown of the cap-binding complex also increases flu transcription, we speculate that the cap-binding complex, recruited by NELF[65,66,81], competes with the flu polymerase for binding to nascent mRNA caps (Figure 7A). Loss of NELF may expand the window in which capped mRNAs are available for flu polymerase binding by delaying both association of the cap-binding complex as well as the transition of RNA polymerase II to productive elongation[60]. However, NELF impacts other aspects of host transcription and cellular physiology, which may also contribute to the effects on flu. Further studies on the mechanism behind the impact of NELF on flu transcription could yield additional insights into the requirements (e.g., timing, binding, etc.) for cap-snatching.

Many previous studies have demonstrated the importance of *de novo* viral RNA for interferon induction by flu[23,84]. For example, previous work from our lab showed that interferon induction by defective viral particles can be increased by complementation, allowing replication of the defective genomes[67]. We have also seen that viral genome replication is essential for the enhanced interferon induction observed in the absence of NS1, suggesting that NS1 protects *de novo* viral ligands[17]. Our finding, in the context of NELF depletion, that increased transcription leads to an increase in interferon induction demonstrates that flu transcription is not only critical but also rate-limiting for the interferon response.

Notably, we found that flu transcription also contributes to interferon induction when viral replication was not permitted. Although genome replication products have been generally regarded as the primary influenza ligand, our finding is consistent with previous work from Richard Randall's group, which also demonstrated transcription-dependent, replication-independent interferon induction[84]. These experiments relied on cycloheximide to prevent viral replication and actinomycin D to prevent host and viral transcription. While both of these drugs have pleiotropic effects, our work supports their conclusions. We have shown that replication-incompetent virus, even in the absence of cycloheximide, induces interferon, and inhibitors specific to flu cap-snatching largely block this interferon expression. Thus, we conclude that influenza transcription-dependent processes, independent of genome replication, contribute to interferon induction (Figure 7B).

Determining which flu RNA(s) are the relevant immunostimulatory ligands in flu infection remains to be clarified. Both transcription and replication have been conclusively shown to be critical steps for interferon induction. Since both of these processes support the other, it remains unknown to what extent they each contribute to the interferon response by directly generating ligands (Figure 7B). Influenza genomes are regarded as the canonical RIG-I ligand, and genome replication also provides more substrates for transcription. Here, we show that transcription itself contributes to interferon induction, at least in the case of defective genomes, which are abundant even in "wild-type" flu populations[85,86]. This may explain why some defective viral particles induce interferon at such high levels, despite only having 8 viral genomes in the entire cell. However, it is unclear what the transcription-dependent, replication-independent ligand(s) may be, as it seems unlikely that flu mRNAs, which are capped and polyadenylated like host mRNAs, would activate RIG-I. Recent work by the te Velthuis lab demonstrated that the flu polymerase can generate capped cRNAs (ccRNAs), which in complex with other small viral RNAs contribute to the interferon response[87]. Generation of ccRNAs would likely require cap-snatching and may be the transcription-dependent ligand we observe here. We also note that baloxavir does not fully block the RNA generation or interferon induction enhanced by NELF depletion, so it is possible that in this context other aberrant RNAs are being generated that may trigger the interferon reponse (Figure 5A-B,E).

In conclusion, a CRITR-seq screen for regulators of interferon expression led us to the finding that components of the host transcription machinery – NELF and the cap-binding complex – modulate the rate of flu transcription. From our screen, we conclude that the concentration of viral ligands is a major factor driving the magnitude of the interferon response. Specifically, we found that flu transcription is both critical and rate-limiting for interferon induction, and can even contribute to the interferon response in the absence of viral replication. In the future, we hope the CRITR-seq platform will be useful to other studies of phenotypes related to gene expression, simply by swapping out the interferon promoter we used here for another promoter of interest.

Methods

KEY RESOURCES TABLE

RESOURCE AVAILABILITY

Lead contact

Further information and requests for resources and reagents should be directed to and will be fulfilled by the Lead Contact, Alistair B. Russell (a5russell@ucsd.edu).

Materials availability

All unique/stable reagents generated in this study are available from the lead contact without restriction.

Data and code availability

- Processed sequencing data have been deposited at Gene Expression Ominbus (GEO) as GEO: GSE281730 and are publicly available as of the date of publication.
- All original code, as well as qPCR data, have been deposited at `https://github.com/acvicary/CRITRseq_Interferon_Flu` and are publicly available at [DOI] as of the date of publication.
- Any additional information required to reanalyze the data reported in this paper is available from the lead contact upon request.

EXPERIMENTAL MODEL DETAILS

Cells

The following cell lines were used in this study: HEK293T (human embryonic kidney, female; ATCC CRL-3216), MDCK-SIAT1 (variant of the Madin Darby canine kidney cell line overexpressing SIAT1, female cocker spaniel; Sigma-Aldrich 05071502), and A549 (human lung epithelial carcinoma, male; ATCC CCL-185).

A549 type III interferon reporter line was previously described[9].

A clonal A549 cell line constitutively expressing Cas9 (A549-Cas9-mCherry) was generated by transducing A549 cells with a lentiviral vector containing Cas9 under the control of a CMV promoter (plasmid sequence in File S1). The mCherry sequence is connected to the Cas9 mRNA by a p2A linker. Cells were validated to be free of replication-competent lentivirus via qPCR for VSV-G. Single cells containing the Cas9 expression construct were isolated by fluorescence-activated cell sorting for mCherry-positive cells. The final clonal line was validated by flow cytometry to have unimodal, high levels of mCherry expression.

An A549 RIG-I-knockout cell line was generated by transfecting A549 cells with a Cas9 ribonucleoprotein complex, using a CRISPR RNA (crRNA) targeting RIG-I exon 1 (IDT Alt-R CRISPR-Cas9 crRNA Hs.Cas9.DDX58.1.AA, Table S2). Single cells were isolated by dilution cloning to generate a clonal line. Residual RIG-I protein expression in this cell line is shown in Figure S8.

Cells were cultured in D10 media (Dulbecco's Modified Eagle Medium supplemented with 10% heat-inactivated fetal bovine serum and 2 mM L-Glutamine) in a 37°C incubator with 5% CO2. The parental A549 cell line used to make the type III interferon reporter line, A49-Cas9-mCherry line, and RIG-I-knockout line was authenticated using the ATCC STR profiling service. Cell lines were tested for mycoplasma using the LookOut Mycoplasma PCR Detection Kit (Sigma-Aldrich) with JumpStart Taq DNA Polymerase (Sigma-Aldrich), or using the MycoStrip® Mycoplasma Detection Kit (InvivoGen, rep-mys-20).

Viruses

Wild-type A/WSN/1933 (H1N1) influenza virus was created by reverse genetics using plasmids pHW181-PB2, pHW182-PB1, pHW183-PA, pHW184-HA, pHW185-NP, pHW186-NA, pHW187-M, pHW188-NS[88]. Genomic sequence of this virus is provided in File S2. HEK293T and MDCK-SIAT1 cells were seeded in an 8:1 coculture and transfected using BioT (Bioland Scientific, LLC) 24 hours later with equimolar reverse genetics plasmids. 24 hours post-transfection, D10 media was changed to Influenza Growth Medium (IGM, Opti-MEM supplemented with 0.04% bovine serum albumin fraction V, 100 μg/mL of $CaCl_2$, and 0.01% heat-inactivated fetal bovine serum). 24 hours after the media change, viral supernatant was collected, centrifuged at 300g for 4 minutes to remove cellular debris, and aliquoted into cryovials to be stored at -80°C. Thawed aliquots were titered by $TCID_{50}$ on MDCK-SIAT1 cells, and calculated using the Reed and Muench formula[89]. To generate a viral population with a low abundance of defective genomes, the virus generated by reverse genetics was then expanded by infecting 3×10^6 MDCK-SIAT1 cells in a 10 cm plate at an infectious MOI of 0.01. Viral supernatant was harvested at 36 hours post-infection, stored, and titered in the same way as the original virus.

$NS1_{stop}$ and $NS1_{mut}$ viruses were generated by reverse genetics using the same plasmids for genome segments 1-7 of the A/WSN/1933 WT virus, but replacing pHW188-NS with a variant NS sequence of pHW188-NS ($NS1_{stop}$) or of pHW198 ($NS1_{mut}$). These variant sequences have 3 stop codons early in the open reading frame of NS1, and the sequences are included in File S2. HEK293T cells were cocultured with MDCK-SIAT1 cells constitutively expressing NS1, and the coculture was transfected with the 8 reverse genetics plasmids as well as a pHAGE2 plasmid containing the gene for WSN-NS1 under the control of the constitutive CMV promoter. D10 was changed to IGM 24 hours post-transfection, and virus was harvested 72 ($NS1_{stop}$) or 52 ($NS1_{mut}$) hours post-transfection. Thawed aliquots were titered by $TCID_{50}$ on MDCK-SIAT1 cells constitutively expressing NS1, or by qPCR against the viral segment HA.

To generate $PB1_{455:350}$[67], HEK293T cells were cocultured with MDCK-SIAT1 cells constitutively expressing PB1. The coculture was transfected with all reverse-genetics plasmids encoding A/WSN/1933 except for a variant of pHW182-PB1 with the indicated deletion (File S2), and a construct expressing PB1 under control of a constitutive promoter in the pHAGE2 vector. D10 was changed to IGM 24 hours post-transfection, and virus was harvested 72 hours after the media change. This virus was titered on MDCK-SIAT1 cells constitutively expressing PB1.

To generate a high-defective wild-type virus population[17], reverse-genetics was performed with the 8 WSN plasmids in every well of a 96-well plate. After 48h, 10 μL of supernatant was transferred to fresh wells, each seeded with 10,000 MDCK-SIAT1 cells. After 48h, 10 μL of that supernatant was transferred to fresh wells, each seeded with 10,000 MDCK-SIAT1 cells. After 48h, all supernatants were harvested, pooled, and clarified, to generate one biological replicate viral population. This virus was titered by $TCID_{50}$ on MDCK-SIAT1 cells, and by qPCR against the viral segment HA.

METHOD DETAILS

Genome-wide CRITR-seq screen

Guides from the Human Genome-Scale CRISPR Knockout (GeCKO) v2 Pooled Library[42] (Addgene Pooled Libraries #1000000048, #1000000049) were cloned into the CRITR-seq vector. To minimize jackpotting from PCR, gRNAs were amplified from GeCKO half-libraries A and B in 8 (Library A) or 7 (Library B) separate 20-cycle PCR reactions, pooled by library, and purified by gel extraction. See Table S3 for primers used in PCR reactions. gRNAs were inserted into the CRITR-seq vector backbone (plasmid sequence in File S3) by Gibson assembly using NEBuilder HiFi DNA Assembly Master Mix (New England Biolabs, E2621), with a 15:1 insert:backbone molar ratio and a 1 hour incubation. DNA $>\sim$1000 bp was purified from the reaction mix using ProNex Size-Selective Purification System magnetic beads (Promega NG2002) at 1x bead volumes, and electroporated into ElectroMAX^{TM} Stbl4^{TM} Competent Cells (Invitrogen 11635018) to achieve at least 10x as many colonies as guides for each half-library. Colonies were scraped from plates, incubated in 100 mL LB at 30°C for 1 hour with shaking, and plasmids were purified by midiprep. When needed, CRITR-seq plasmid libraries were amplified by electroporating 4 ng of the original generated library.

To generate lentiviral libraries, $6.32\text{x}10^6$ HEK293T cells were seeded in D10 in each of 2 T75 flasks to achieve $\sim$80% confluence. Cells in each flask were transfected with a total of 10.27 μg DNA combined from CRITR-seq libraries A and B, proportional to the number of guides per library. Plasmid libraries were transfected using Lipofectamine 3000 and P3000, along with lentiviral helper plasmids HDM-Hgpm2 (Addgene #204152), HDM-tat1b (Addgene #204154), pRC-CMV-Rev1 (Addgene #164443), and HDM_VSV_G (Addgene #204156), at 10.27 μg divided equally between them. 6 hours post-transfection, the media was changed to fresh D10. 24 hours post-transfection, virus was harvested and stored at 4°C, replacing the media. 50 hours post-transfection, virus was harvested again, pooled with the first harvest, and centrifuged at 300 g for 4 minutes to remove cell debris. Aliquots were stored at -80°C. The CRITR-seq vector does not contain a selectable marker, so we titered the lentiviral libraries by flow cytometry, taking advantage of the zsGreen marker under the control of the *IFNL1* promoter. A549 cells were seeded at 67,500 cells/well in a 24-well plate and transduced with serial dilutions of lentivirus from 1x to 256x, with 3 replicates per dilution. 24 hours post-transduction, the media was replaced with fresh D10. 48 hours post-transduction, cells were seeded for infection at 70,000 cells/well. Cells were infected at a saturating infectious MOI of 2.8 using an influenza variant that induces interferon in $\sim$100% of infected cells, and fixed with formaldehyde 13 hours post-infection. The percent of zsGreen+ cells measured by flow cytometry was considered to be the fraction of cells that had integrated the CRITR-seq vector. We used the dilutions which appeared to be in the linear range to calculate the transduction units (TU) per μL for each library.

To generate libraries of edited cells, $2.666\text{x}10^6$ A549-Cas9-mCherry cells were seeded in each of 3 T75 flasks. Cells were transduced with a CRITR-seq lentiviral library at an MOI of 1.5, using 8 μg/mL polybrene (Sigma-Aldrich, TR-1003-G). This is a higher MOI than is typical for CRISPR screens, as we assumed that most gene edits would not impact interferon expression. With this MOI and cell count, we were transducing cells with $\sim$100x coverage of the gRNAs from the GeCKO library. 24 hours post-transduction, the media was changed to fresh D10, and cells were passaged for 10 days, maintaining over 100x coverage of the libraries at each passage. On day 10 post-transduction, cells were seeded at $7\text{x}10^6$ cells per 15 cm plate in 12 plates for $\sim$1000x coverage of gRNAs. The day following seeding, D10 was replaced with IGM for infection with $NS1_{mut}$ at a genome-corrected MOI of 2. 8 hours post-infection, cells from all plates were trypsinized and pooled. Half of the cells were lysed in genomic DNA lysis buffer and processed for genomic DNA extraction (Monarch Spin gDNA Extraction Kit; New England Biolabs, T3010S), and half of the cells were lysed in RNA lysis buffer and processed for RNA extraction (Monarch Total RNA Miniprep Kit; New England Biolabs, T2010S).

To prepare genomic DNA for amplicon sequencing, 50 μg gDNA was split into 20 50-μL PCR reactions. Assuming 6 pg gDNA per cell and 1.5 guides per cell, this would give $\sim$100x coverage of gRNAs. We used Q5 Hot Start High-Fidelity 2X Master Mix and primers specific for a 194 base pair region of the CRITR-seq vector containing the gRNA sequence (Table S3). Amplicons were bead purified using 3x bead volumes, and 5% of the bead-cleaned product was amplified by a second PCR using primers containing partial Illumina adapters (Table S3). Amplicons were purified in a 2-sided bead clean-up, and DNA concentrations were determined by Qubit. Final Illumina indices were added by PCR for each sample, using 10 ng of amplicon. Indexing primers were from IDT for Illumina DNA/RNA unique dual indexes (Set A, #20026121). PCR reactions were bead purified using 2x bead volumes and verified by running on an agarose gel. Final DNA concentrations were determined by Qubit before pooling equal amounts for sequencing.

To prepare mRNA for amplicon sequencing, we reverse transcribed 1 μg of total RNA using oligo(dT) primers and the Superscript III First-Strand Synthesis SuperMix kit (Invitrogen, 18080400) according to the manufacturer's protocol. 10% of the total RT reaction was amplified in each of 5 PCR reactions. PCR amplification and indexing was performed with the same steps and primers as used for genomic DNA preparation.

The entire process from PCR to final gDNA/RNA extraction and sequencing preparation was repeated 3 times for 3 independent biological replicates of the CRITR-seq screen.

Individual gene knockout by CRISPR/Cas9

Individual gene knockouts were performed by CRISPR ribonucleoprotein (crRNP) transfection, using the Alt-R^{TM} S.p. HiFi Cas9 Nuclease V3 (Integrated DNA Technologies, 1081060). Alt-R^{TM} CRISPR-Cas9 tracrRNA (Integrated DNA Technologies, 1073189) and the specific crRNA were complexed together by mixing at equimolar concentration to a final concentration of 1 μM in Nuclease-Free Duplex Buffer (Integrated DNA Technologies, 0000934164) and heating at 95°C for 5 minutes. The RNP complex was formed by mixing the crRNA-tracrRNA duplex and Cas9 to a final concentration of 60 nM each in Opti-MEM and incubating 5 minutes at room temperature. The crRNP complex was reverse transfected into 160,000 A549 cells in a 24-well plate using Lipofectamine RNAiMAX (Invitrogen, 100014472), with a final concentration of 6 nM crRNP. Experiments were performed 10 days post-transfection to allow sufficient time for editing and protein turnover.

siRNA knockdown

All siRNAs were Ambion Silencer Select siRNAs (Life Technologies Corporation). Catalog numbers are provided in Table S4.

For *NELFB* knockdown, 100,000 A549 cells/well in a 24-well plate were each reverse-transfected in 500 μL D10 with 50 μL Opti-MEM, 1.5 μL of Lipofectamine 3000 (Invitrogen, L3000001), and 0.25 μL of 10 μM siRNA. Media was replaced with fresh D10 24 hours post-transfection. 4 days after transfection, cells were trypsinized and again reverse-transfected with siRNA. siRNA treatment was repeated again 4 days after the second transfection to seed for infection at 100,000 cells/well. Influenza infection or poly(I:C) transfection was performed 24 hours after the third transfection.

siRNA sequence and protocol for *NCBP1* knockdown were based on the methods from Gebhardt, et al.[90]. 100,000 A549 cells/well in a 6-well plate were each reverse-transfected in 2 mL D10 with 250 μL Opti-MEM, 7.5 μL of Lipofectamine RNAiMAX, and 2.5 μL of 10 μM siRNA. Media was replaced with fresh D10 24 hours post-transfection. 48 hours after transfection, cells were trypsinized and re-treated with siRNA, at 200,000 cells/well in a 6-well plate. 24 hours after the second transfection, cells were trypsinized and re-seeded in a 24-well plate at 50,000 cells/well, with no additional siRNA treatment. Influenza infection was performed 24 hours after seeding (96 hours after the first transfection).

poly(I:C) transfection

500 ng poly(I:C) (Fisher Scientific, 42-871-0) was complexed with 1.5 μL Lipofectamine 3000 in 50 μL Opti-MEM. 5 μL of the complex (containing 50 ng poly(I:C)) was added to each well of a 24-well plate, with 100,000 A549 cells/well. Cells were lysed for RNA extraction 8 hours post-transfection.

qPCR

Infections were performed on cells seeded 24 hours prior to infection, changed to IGM at time of infection. RNA was purified from infected cells or viral supernatant using the Monarch Total RNA Miniprep kit from New England Biolabs or the Zymo Research Quick-RNA Miniprep kit, following manufacturer's protocol. cDNA from 100 ng purified RNA was generated using the High Capacity cDNA Reverse Transcription Kit (Applied Biosystems, 4368814) with random hexamer primers, oligo(dT) primers (for initial screen validation, Figure 3B), or universal influenza primers (for viral titer from supernatant, Figure 4F, S7) according to the manufacturer's protocol. When 100 ng purified RNA was not available (in viral titer experiments), we used a final lysate concentration of 10% of the reaction volume. qPCR was performed using Luna Universal qPCR Master Mix (New England Biolabs, M3003) with manufacturer's suggested reaction conditions. Primers for all qPCR analyses are listed in Table S3. Code generating graphs in manuscript can be found at `https://github.com/acvicary/CRITRseq_Interferon_Flu`.

Inhibitor treatment

Inhibitors were diluted in IGM to final concentrations of 10 nM or 100 nM for baloxavir acid, 100 nM for pimodivir, or

50 μg/mL for cycloheximide. At time of infection, or 2 hours pre-infection for pimodivir experiments, 100,000 A549 cells in a 24-well plate were treated by replacing D10 from seeding with 500μL IGM with or without the indicated inhibitors.

Flow cytometry

Indicated cells were seeded 24 hours prior to infection, changed to IGM at the time of infection, and trypsinized and resuspended in PBS supplemented with 2% of heat-inactivated fetal bovine serum (FBS) 13 hours post-infection. For M2 staining, a mouse monoclonal antibody (Invitrogen, MA1-082) was used at a concentration of 5 μg/mL. Secondary antibody staining was performed with goat anti-mouse IgG conjugated to allophycocyanin (Invitrogen, A-865) at a concentration of 5 μg/mL. Cells were fixed with BD Cytofix/Cytoperm (BD Biosciences, 51-2090KZ), following manufacturers instructions.

FlowJo was used to generate a gate excluding debris prior to export to a csv. Data for non-debris events were analyzed using custom Python scripts, which can be found at `https://github.com/acvicary/CRITRseq_Interferon_Flu`. Uninfected controls were used to set empirical gates for influenza staining and interferon reporter positivity at a 99.9% exclusion criteria.

5' Rapid Amplification of cDNA Ends (RACE)

To identify the sequences of the 5' terminal ends of the viral mRNA upon NELFB knockdown, cells were treated with either no, non-targeting, or one of two *NELFB* siRNAs for 9 days according to the *NELFB* siRNA knockdown procedure described above. Cells were infected with $\mathrm{NS1_{mut}}$ at a genome-corrected MOI of 2 for 8 hours before lysing cells and extracting RNA using the Monarch Total RNA Miniprep Kit from New England Biolabs. Samples were reverse transcribed with the Template Switching RT Enzyme Mix (New England Biolabs, #M0466) according to the manufacturer's protocol. In brief, sample RNA was annealed with oligo(dT) primers and then reverse transcribed with the template-switching oligo (TSO, Table S3), which contains mixed ribonucleotides at the third from final position, a locked nucleic acid at the final position, and a 5' biotin modification to prevent spurious additional concatemerization, similar to that from Picelli et al.[91,92]. Amplification of the 5' terminal ends of the flu mRNA were performed in separate reactions using a TSO-specific amplification primer and segment-specific mRNA primers (Table S3), using Q5 Hot Start High-Fidelity 2X Master Mix. Amplification was repeated with primers containing partial Illumina i5 and i7 adapters (common TSO partial adapter and segment-specific primers in Table S3). Amplicons were bead purified, pooled by sample, and verified on a gel. DNA concentration was determined by Qubit, and final Illumina indices were added by PCR for each sample, using 1.5 ng of amplicon. Indexing primers were from IDT for Illumina DNA/RNA unique dual indexes (Set A, #20026121). PCR reactions were bead purified, and final DNA concentrations were determined by Qubit before pooling equal amounts for sequencing.

Single-cycle viral titer

A549 cells were seeded at 100,000 cells/well in a 24 well plate. 24 hours after seeding, the media was replaced with IGM and infected with WT WSN at an infectious MOI of 2. 2 hours post-infection, the media was replaced with fresh IGM. 14 hours post-infection, supernatant was collected and centrifuged at 300g for 4 minutes to clear cell debris. 40 μL of supernatant was mixed with 360 μL RNA lysis buffer for qPCR analysis. Cells were also lysed for RNA extraction and qPCR analysis.

Western blot

Cells were seeded in a 24-well plate at 100,000 cells/well 24 hours prior to infection. Cells were infected with $\mathrm{NS1_{mut}}$ at a genome-corrected MOI of 5 for 24 hours. Infected cells were then washed three times with PBS and lysed in 1x Laemmli Sample Buffer (Bio-Rad #1610747) containing 100mM DTT. Lysate was boiled at 100°C for 5 minutes and resolved by SDS-PAGE (Bio-Rad #4561024) and transferred onto a nitrocellulose membrane. The membrane was blocked with PBST buffer (1x PBS with 0.1% Tween-20) containing 5% nonfat dry milk for 1 hour at room temperature. The membrane was incubated overnight at 4°C with anti-RIG-I monoclonal antibody (Cell Signaling Technology, 3743T; 1:1000 dilution in PBST) or anti-β-actin monoclonal antibody (Cell Signaling Technology, 8457T; 1:1000 dilution in PBST) as a loading control. The membrane was then incubated for 1 hour at room temperature with HRP-linked anti-rabbit IgG secondary antibody (Cell Signaling Technology, 7074P2; 1:3000 dilution in PBST) to detect primary antibody staining. HRP-conjugates were visualized using the Clarity Western ECL Substrate kit (Bio-Rad #1705060S).

QUANTIFICATION AND STATISTICAL ANALYSIS

Amplicon sequencing and MAGeCK analysis

gRNA sequences were determined for reads with perfect matches to the CRITR-seq vector for the 10 nucleotides upstream and 13 nucleotides downstream of the gRNA. gRNA sequences with perfect matches to a guide from the GeCKO library were kept and assigned. A file containing the counts for each gRNA in each replicate for both gDNA and mRNA was compiled, and guides with less than 25 reads in the gDNA for any replicate were dropped. This file was used as the input file for Model-based Analysis of Genome-wide CRISPR/Cas9 Knockout (MAGeCK)[41].

For MAGeCK analysis, gDNA and mRNA from the same replicate were considered paired samples, and the non-targeting gRNAs with at least 25 counts in the gDNA for all replicates were used for normalization and generating the null distribution for robust ranking aggregation (RRA). The following command was run using MAGeCK version 0.5.9.5:

```
mageck test -k mageckCounts_threshold25.txt -t Flu1_RNA,Flu2_RNA,Flu3_RNA -c
Flu1_DNA,Flu2_DNA,Flu3_DNA –paired –norm-method control –control-sgrna nontarget.txt
```

The input files above were generated with Python scripts provided at `https://github.com/acvicary/CRITRseq_Interferon_Flu`.

After MAGeCK analysis, genes with a column was added to the gene summary file with the UMI count for each gene, summed across all cells, from a previous single cell sequencing dataset generated from A549s after influenza infection[17]. Genes with no expression in A549s (total UMI=0) were dropped from further analysis.

5' RACE sequencing analysis

Reads containing a perfect match to the TSO were searched for the first 20 bases of the mRNA sequence from each of the 8 flu genome segments. Reads with at least 15 nucleotide identity were considered matching to that flu mRNA. The sequence downstream of the TSO and upstream of the +1 position of the viral mRNA sequence was considered to be the cap sequence. We note that the length of this sequence could be +/-1 compared to the true length of the cap sequence due to the variable number of non-templated nucleotides added by the reverse transcriptase after it reaches the 5' end of the RNA. A large number of duplicate cap sequences indicated that there was substantial bottlenecking in the sample preparation process, so only unique cap sequences were kept for analysis. Median cap sequence length for each sample was 12 nucleotides. Distribution of cap sequence lengths were plotted, excluding the top 2% of lengths. Distributions were compared by ANOVA and post hoc Tukey's test, $n=8$, $p<0.05$, $q<0.05$.

Statistical analyses

All experiments were performed in biological triplicate, except for 5' RACE to determine cap lengths which used 2 biological replicates per treatment condition. qPCR experiments were performed with technical duplicate. Multiple comparisons were performed using one-way ANOVA with a post hoc Tukey's test. Pairwise comparisons were performed with one- or two-tailed t-tests, as indicated. For panels testing multiple hypotheses, the Benjamini-Hochberg multiple hypothesis correction was applied. Alpha was set to 0.05 for all significance testing. Figures were assembled in Adobe Illustrator (28.5).

Acknowledgments

This work was supported by the NIGMS of the NIH under grant R35GM147031 awarded to ABR. ACV was supported by the NIGMS of the NIH under grant T32GM133351.

Author Contributions

A.B.R. and A.C.V. designed experiments, A.B.R., A.C.V, S.N.Z.J., M.M., S.S., L.K.C., and J.S.P performed experiments, A.B.R and A.C.V performed data analysis, A.B.R and A.C.V. conceived this study, discussed results, and wrote the manuscript.

Declaration of Interests

The authors declare no competing interests.

References

1. Park, A. & Iwasaki, A. Type I and Type III Interferons – Induction, Signaling, Evasion, and Application to Combat COVID-19. *Cell Host & Microbe* **27,** 870–878. doi:10.1016/j.chom.2020.05.008 (June 2020).
2. Lazear, H. M., Schoggins, J. W. & Diamond, M. S. Shared and Distinct Functions of Type I and Type III Interferons. English. *Immunity* **50.** Publisher: Elsevier, 907–923. doi:10.1016/j.immuni.2019.03.025 (Apr. 2019).
3. McNab, F., Mayer-Barber, K., Sher, A., Wack, A. & O'Garra, A. Type I interferons in infectious disease. en. *Nature Reviews Immunology* **15.** Publisher: Nature Publishing Group, 87–103. doi:10.1038/nri3787 (Feb. 2015).
4. Zawatzky, R., De Maeyer, E. & De Maeyer-Guignard, J. Identification of individual interferon-producing cells by in situ hybridization. *Proceedings of the National Academy of Sciences* **82.** Publisher: Proceedings of the National Academy of Sciences, 1136–1140. doi:10.1073/pnas.82.4.1136 (Feb. 1985).
5. Hu, J. *et al.* Chromosome-specific and noisy IFNB1 transcription in individual virus-infected human primary dendritic cells. *Nucleic Acids Research* **35,** 5232–5241. doi:10.1093/nar/gkm557 (Aug. 2007).
6. Chen, S. *et al.* Heterocellular induction of interferon by negative-sense RNA viruses. *Virology* **407,** 247–255. doi:10.1016/j.virol.2010.08.008 (Nov. 2010).
7. Zhao, M., Zhang, J., Phatnani, H., Scheu, S. & Maniatis, T. Stochastic Expression of the Interferon-β Gene. en. *PLOS Biology* **10.** Publisher: Public Library of Science, e1001249. doi:10.1371/journal.pbio.1001249 (Jan. 2012).
8. Rand, U. *et al.* Multi-layered stochasticity and paracrine signal propagation shape the type-I interferon response. *Molecular Systems Biology* **8.** Publisher: John Wiley & Sons, Ltd, 584. doi:10.1038/msb.2012.17 (Jan. 2012).
9. Russell, A. B., Elshina, E., Kowalsky, J. R., Te Velthuis, A. J. W. & Bloom, J. D. Single-Cell Virus Sequencing of Influenza Infections That Trigger Innate Immunity. en. *Journal of Virology* **93** (ed Pfeiffer, J. K.) e00500–19. doi:10.1128/JVI.00500-19 (July 2019).
10. Patil, S. *et al.* Single-cell analysis shows that paracrine signaling by first responder cells shapes the interferon-β response to viral infection. eng. *Science Signaling* **8,** ra16. doi:10.1126/scisignal.2005728 (Feb. 2015).
11. Zhang, Q. *et al.* Inborn errors of type I IFN immunity in patients with life-threatening COVID-19. *Science* **370.** Publisher: American Association for the Advancement of Science, eabd4570. doi:10.1126/science.abd4570 (Oct. 2020).
12. Meyts, I. & Casanova, J.-L. Viral infections in humans and mice with genetic deficiencies of the type I IFN response pathway. en. *European Journal of Immunology* **51,** 1039–1061. doi:10.1002/eji.202048793 (2021).
13. Crow, Y. J. & Stetson, D. B. The type I interferonopathies: 10 years on. en. *Nature Reviews Immunology* **22.** Publisher: Nature Publishing Group, 471–483. doi:10.1038/s41577-021-00633-9 (Aug. 2022).
14. Kato, H. *et al.* Length-dependent recognition of double-stranded ribonucleic acids by retinoic acid–inducible gene-I and melanoma differentiation–associated gene 5. *Journal of Experimental Medicine* **205,** 1601–1610. doi:10.1084/jem.20080091 (June 2008).
15. Iwasaki, A. & Pillai, P. S. Innate immunity to influenza virus infection. en. *Nature Reviews Immunology* **14.** Publisher: Nature Publishing Group, 315–328. doi:10.1038/nri3665 (May 2014).
16. García-Sastre, A. *et al.* Influenza A Virus Lacking the NS1 Gene Replicates in Interferon-Deficient Systems. *Virology* **252,** 324–330. doi:10.1006/viro.1998.9508 (Dec. 1998).
17. Vicary, A. C. *et al.* Maximal interferon induction by influenza lacking NS1 is infrequent owing to requirements for replication and export. en. *PLOS Pathogens* **19.** Publisher: Public Library of Science, e1010943. doi:10.1371/journal.ppat.1010943 (Apr. 2023).

18. Pflug, A., Lukarska, M., Resa-Infante, P., Reich, S. & Cusack, S. Structural insights into RNA synthesis by the influenza virus transcription-replication machine. *Virus Research. Viral polymerases* **234,** 103–117. doi:10.1016/j.virusres.2017.01.013 (Apr. 2017).
19. Rehwinkel, J. *et al.* RIG-I Detects Viral Genomic RNA during Negative-Strand RNA Virus Infection. English. *Cell* **140.** Publisher: Elsevier, 397–408. doi:10.1016/j.cell.2010.01.020 (Feb. 2010).
20. Marcus, P. I., Rojek, J. M. & Sekellick, M. J. Interferon Induction and/or Production and Its Suppression by Influenza A Viruses. *Journal of Virology* **79.** Publisher: American Society for Microbiology, 2880–2890. doi:10.1128/jvi.79.5.2880-2890.2005 (Mar. 2005).
21. Baum, A., Sachidanandam, R. & García-Sastre, A. Preference of RIG-I for short viral RNA molecules in infected cells revealed by next-generation sequencing. *Proceedings of the National Academy of Sciences* **107.** Publisher: Proceedings of the National Academy of Sciences, 16303–16308. doi:10.1073/pnas.1005077107 (Sept. 2010).
22. Tapia, K. *et al.* Defective Viral Genomes Arising In Vivo Provide Critical Danger Signals for the Triggering of Lung Antiviral Immunity. en. *PLOS Pathogens* **9.** Publisher: Public Library of Science, e1003703. doi:10.1371/journal.ppat.1003703 (Oct. 2013).
23. Te Velthuis, A. J. W. *et al.* Mini viral RNAs act as innate immune agonists during influenza virus infection. en. *Nature Microbiology* **3.** Publisher: Nature Publishing Group, 1234–1242. doi:10.1038/s41564-018-0240-5 (Nov. 2018).
24. Killip, M. J., Fodor, E. & Randall, R. E. Influenza virus activation of the interferon system. *Virus Research. Special Issue: Cell response to viral infection* **209,** 11–22. doi:10.1016/j.virusres.2015.02.003 (Nov. 2015).
25. Enoch, T., Zinn, K. & Maniatis, T. Activation of the Human β-Interferon Gene Requires an Interferon-Inducible Factor. *Molecular and Cellular Biology* **6.** Publisher: Taylor & Francis _eprint: https://doi.org/10.1128/mcb.6.3.801-810.1986, 801–810. doi:10.1128/mcb.6.3.801-810.1986 (Mar. 1986).
26. West, A. P. *et al.* Mitochondrial DNA stress primes the antiviral innate immune response. en. *Nature* **520.** Publisher: Nature Publishing Group, 553–557. doi:10.1038/nature14156 (Apr. 2015).
27. Vabret, N. *et al.* Y RNAs are conserved endogenous RIG-I ligands across RNA virus infection and are targeted by HIV-1. *iScience* **25,** 104599. doi:10.1016/j.isci.2022.104599 (July 2022).
28. King, C. R. *et al.* Pathogen-driven CRISPR screens identify TREX1 as a regulator of DNA self-sensing during influenza virus infection. *Cell Host & Microbe* **31,** 1552–1567.e8. doi:10.1016/j.chom.2023.08.001 (Sept. 2023).
29. Ivashkiv, L. B. & Donlin, L. T. Regulation of type I interferon responses. en. *Nature Reviews Immunology* **14.** Publisher: Nature Publishing Group, 36–49. doi:10.1038/nri3581 (Jan. 2014).
30. Ma, M., Jiang, W. & Zhou, R. DAMPs and DAMP-sensing receptors in inflammation and diseases. English. *Immunity* **57.** Publisher: Elsevier, 752–771. doi:10.1016/j.immuni.2024.03.002 (Apr. 2024).
31. Russell, A. B., Trapnell, C. & Bloom, J. D. Extreme heterogeneity of influenza virus infection in single cells. *eLife* **7** (ed Chakraborty, A. K.) Publisher: eLife Sciences Publications, Ltd, e32303. doi:10.7554/eLife.32303 (Feb. 2018).
32. Sun, J. *et al.* Single cell heterogeneity in influenza A virus gene expression shapes the innate antiviral response to infection. en. *PLOS Pathogens* **16.** Publisher: Public Library of Science, e1008671. doi:10.1371/journal.ppat.1008671 (July 2020).
33. Gaidt, M. M. *et al.* Self-guarding of MORC3 enables virulence factor-triggered immunity. en. *Nature* **600.** Publisher: Nature Publishing Group, 138–142. doi:10.1038/s41586-021-04054-5 (Dec. 2021).
34. Carlson, R. J., Leiken, M. D., Guna, A., Hacohen, N. & Blainey, P. C. A genome-wide optical pooled screen reveals regulators of cellular antiviral responses. *Proceedings of the National Academy of Sciences* **120.** Publisher: Proceedings of the National Academy of Sciences, e2210623120. doi:10.1073/pnas.2210623120 (Apr. 2023).
35. Lumb, J. H. *et al.* DDX6 Represses Aberrant Activation of Interferon-Stimulated Genes. English. *Cell Reports* **20.** Publisher: Elsevier, 819–831. doi:10.1016/j.celrep.2017.06.085 (July 2017).
36. Harding, A. T., Goff, M. A., Froggatt, H. M., Lim, J. K. & Heaton, N. S. GPER1 is required to protect fetal health from maternal inflammation. *Science* **371.** Publisher: American Association for the Advancement of Science, 271–276. doi:10.1126/science.aba9001 (Jan. 2021).

37. Börold, J. *et al.* BRD9 is a druggable component of interferon-stimulated gene expression and antiviral activity. *EMBO reports* **22.** Publisher: John Wiley & Sons, Ltd, e52823. doi:10.15252/embr.202152823 (Oct. 2021).

38. Muller, R., Meacham, Z. A., Ferguson, L. & Ingolia, N. T. CiBER-seq dissects genetic networks by quantitative CRISPRi profiling of expression phenotypes. *Science* **370.** Publisher: American Association for the Advancement of Science, eabb9662. doi:10.1126/science.abb9662 (Dec. 2020).

39. Sack, L. M., Davoli, T., Xu, Q., Li, M. Z. & Elledge, S. J. Sources of Error in Mammalian Genetic Screens. en. *G3: Genes|Genomes|Genetics* **6,** 2781. doi:10.1534/g3.116.030973 (July 2016).

40. Datlinger, P. *et al.* Pooled CRISPR screening with single-cell transcriptome readout. en. *Nature Methods* **14.** Publisher: Nature Publishing Group, 297–301. doi:10.1038/nmeth.4177 (Mar. 2017).

41. Li, W. *et al.* MAGeCK enables robust identification of essential genes from genome-scale CRISPR/Cas9 knockout screens. *Genome Biology* **15,** 554. doi:10.1186/s13059-014-0554-4 (Dec. 2014).

42. Sanjana, N. E., Shalem, O. & Zhang, F. Improved vectors and genome-wide libraries for CRISPR screening. en. *Nature Methods* **11.** Publisher: Nature Publishing Group, 783–784. doi:10.1038/nmeth.3047 (Aug. 2014).

43. Marié, I., Durbin, J. E. & Levy, D. E. Differential viral induction of distinct interferon-α genes by positive feedback through interferon regulatory factor-7. *The EMBO Journal* **17.** Num Pages: 6669 Publisher: John Wiley & Sons, Ltd, 6660–6669. doi:10.1093/emboj/17.22.6660 (Nov. 1998).

44. Sato, M. *et al.* Positive feedback regulation of type I IFN genes by the IFN-inducible transcription factor IRF-7. en. *FEBS Letters* **441.** _eprint: https://onlinelibrary.wiley.com/doi/pdf/10.1016/S0014-5793%2898%2901514-2, 106–110. doi:10.1016/S0014-5793(98)01514-2 (1998).

45. Li, B. *et al.* Genome-wide CRISPR screen identifies host dependency factors for influenza A virus infection. en. *Nature Communications* **11.** Publisher: Nature Publishing Group, 164. doi:10.1038/s41467-019-13965-x (Jan. 2020).

46. Joung, J. *et al.* Genome-scale CRISPR-Cas9 Knockout and Transcriptional Activation Screening. en. *Nature protocols* **12,** 828. doi:10.1038/nprot.2017.016 (Mar. 2017).

47. Cadena, C. *et al.* Ubiquitin-Dependent and -Independent Roles of E3 Ligase RIPLET in Innate Immunity. en. *Cell* **177,** 1187–1200.e16. doi:10.1016/j.cell.2019.03.017 (May 2019).

48. Saha, S. K. *et al.* Regulation of antiviral responses by a direct and specific interaction between TRAF3 and Cardif. *The EMBO Journal* **25.** Num Pages: 3263 Publisher: John Wiley & Sons, Ltd, 3257–3263. doi:10.1038/sj.emboj.7601220 (July 2006).

49. Zhao, T. *et al.* The NEMO adaptor bridges the nuclear factor-κB and interferon regulatory factor signaling pathways. en. *Nature Immunology* **8.** Publisher: Nature Publishing Group, 592–600. doi:10.1038/ni1465 (June 2007).

50. Ryzhakov, G. & Randow, F. SINTBAD, a novel component of innate antiviral immunity, shares a TBK1-binding domain with NAP1 and TANK. en. *The EMBO Journal* **26,** 3180. doi:10.1038/sj.emboj.7601743 (June 2007).

51. Au, W. C., Moore, P. A., Lowther, W., Juang, Y. T. & Pitha, P. M. Identification of a member of the interferon regulatory factor family that binds to the interferon-stimulated response element and activates expression of interferon-induced genes. eng. *Proceedings of the National Academy of Sciences of the United States of America* **92,** 11657–11661. doi:10.1073/pnas.92.25.11657 (Dec. 1995).

52. Rehwinkel, J. & Gack, M. U. RIG-I-like receptors: their regulation and roles in RNA sensing. en. *Nature Reviews Immunology* **20.** Publisher: Nature Publishing Group, 537–551. doi:10.1038/s41577-020-0288-3 (Sept. 2020).

53. Yamaguchi, Y. *et al.* NELF, a multisubunit complex containing RD, cooperates with DSIF to repress RNA polymerase II elongation. eng. *Cell* **97,** 41–51. doi:10.1016/s0092-8674(00)80713-8 (Apr. 1999).

54. Narita, T. *et al.* Human Transcription Elongation Factor NELF: Identification of Novel Subunits and Reconstitution of the Functionally Active Complex. en. *Molecular and Cellular Biology* **23,** 1863. doi:10.1128/MCB.23.6.1863-1873.2003 (Mar. 2003).

55. Wu, C.-H. *et al.* NELF and DSIF cause promoter proximal pausing on the hsp70 promoter in Drosophila. en. *Genes & Development* **17.** Company: Cold Spring Harbor Laboratory Press Distributor: Cold Spring Harbor Laboratory Press Institution: Cold Spring Harbor Laboratory Press Label: Cold Spring Harbor Laboratory Press Publisher: Cold Spring Harbor Lab, 1402–1414. doi:10.1101/gad.1091403 (June 2003).

56. Vos, S. M. *et al.* Architecture and RNA binding of the human negative elongation factor. *eLife* **5** (ed Adelman, K.) Publisher: eLife Sciences Publications, Ltd, e14981. doi:10.7554/eLife.14981 (June 2016).
57. Vos, S. M., Farnung, L., Urlaub, H. & Cramer, P. Structure of paused transcription complex Pol II–DSIF–NELF. en. *Nature* **560.** Publisher: Nature Publishing Group, 601–606. doi:10.1038/s41586-018-0442-2 (Aug. 2018).
58. Muse, G. W. *et al.* RNA polymerase is poised for activation across the genome. en. *Nature Genetics* **39.** Publisher: Nature Publishing Group, 1507–1511. doi:10.1038/ng.2007.21 (Dec. 2007).
59. Henriques, T. *et al.* Stable Pausing by RNA Polymerase II Provides an Opportunity to Target and Integrate Regulatory Signals. English. *Molecular Cell* **52.** Publisher: Elsevier, 517–528. doi:10.1016/j.molcel.2013.10.001 (Nov. 2013).
60. DeBerardine, M., Booth, G. T., Versluis, P. P. & Lis, J. T. The NELF pausing checkpoint mediates the functional divergence of Cdk9. en. *Nature Communications* **14.** Publisher: Nature Publishing Group, 2762. doi:10.1038/s41467-023-38359-y (May 2023).
61. Adelman, K. & Lis, J. T. Promoter-proximal pausing of RNA polymerase II: emerging roles in metazoans. en. *Nature Reviews Genetics* **13.** Publisher: Nature Publishing Group, 720–731. doi:10.1038/nrg3293 (Oct. 2012).
62. Mandal, S. S. *et al.* Functional interactions of RNA-capping enzyme with factors that positively and negatively regulate promoter escape by RNA polymerase II. *Proceedings of the National Academy of Sciences* **101.** Publisher: Proceedings of the National Academy of Sciences, 7572–7577. doi:10.1073/pnas.0401493101 (May 2004).
63. Sims, R. J., Belotserkovskaya, R. & Reinberg, D. Elongation by RNA polymerase II: the short and long of it. en. *Genes & Development* **18.** Company: Cold Spring Harbor Laboratory Press Distributor: Cold Spring Harbor Laboratory Press Institution: Cold Spring Harbor Laboratory Press Label: Cold Spring Harbor Laboratory Press Publisher: Cold Spring Harbor Lab, 2437–2468. doi:10.1101/gad.1235904 (Oct. 2004).
64. Krischuns, T., Lukarska, M., Naffakh, N. & Cusack, S. Influenza Virus RNA-Dependent RNA Polymerase and the Host Transcriptional Apparatus. en. *Annual Review of Biochemistry* **90,** 321–348. doi:10.1146/annurev-biochem-072820-100645 (June 2021).
65. Aoi, Y. *et al.* NELF Regulates a Promoter-Proximal Step Distinct from RNA Pol II Pause-Release. eng. *Molecular Cell* **78,** 261–274.e5. doi:10.1016/j.molcel.2020.02.014 (Apr. 2020).
66. Narita, T. *et al.* NELF Interacts with CBC and Participates in 3' End Processing of Replication-Dependent Histone mRNAs. English. *Molecular Cell* **26.** Publisher: Elsevier, 349–365. doi:10.1016/j.molcel.2007.04.011 (May 2007).
67. Mendes, M. & Russell, A. B. Library-based analysis reveals segment and length dependent characteristics of defective influenza genomes. en. *PLOS Pathogens* **17.** Publisher: Public Library of Science, e1010125. doi:10.1371/journal.ppat.1010125 (Dec. 2021).
68. Engelhardt, O. G., Smith, M. & Fodor, E. Association of the Influenza A Virus RNA-Dependent RNA Polymerase with Cellular RNA Polymerase II. *Journal of Virology* **79.** Publisher: American Society for Microbiology, 5812–5818. doi:10.1128/jvi.79.9.5812-5818.2005 (May 2005).
69. Guilligay, D. *et al.* The structural basis for cap binding by influenza virus polymerase subunit PB2. en. *Nature Structural & Molecular Biology* **15.** Publisher: Nature Publishing Group, 500–506. doi:10.1038/nsmb.1421 (May 2008).
70. Martínez-Alonso, M., Hengrung, N. & Fodor, E. RNA-Free and Ribonucleoprotein-Associated Influenza Virus Polymerases Directly Bind the Serine-5-Phosphorylated Carboxyl-Terminal Domain of Host RNA Polymerase II. *Journal of Virology* **90.** Publisher: American Society for Microbiology, 6014–6021. doi:10.1128/jvi.00494-16 (June 2016).
71. Lukarska, M. *et al.* Structural basis of an essential interaction between influenza polymerase and Pol II CTD. en. *Nature* **541.** Publisher: Nature Publishing Group, 117–121. doi:10.1038/nature20594 (Jan. 2017).
72. Plotch, S. J., Bouloy, M., Ulmanen, I. & Krug, R. M. A unique cap(m7GpppXm)-dependent influenza virion endonuclease cleaves capped RNAs to generate the primers that initiate viral RNA transcription. English. *Cell* **23.** Publisher: Elsevier, 847–858. doi:10.1016/0092-8674(81)90449-9 (Mar. 1981).
73. Dias, A. *et al.* The cap-snatching endonuclease of influenza virus polymerase resides in the PA subunit. en. *Nature* **458.** Publisher: Nature Publishing Group, 914–918. doi:10.1038/nature07745 (Apr. 2009).

74. Chan, A. Y., Vreede, F. T., Smith, M., Engelhardt, O. G. & Fodor, E. Influenza virus inhibits RNA polymerase II elongation. *Virology* **351,** 210–217. doi:10.1016/j.virol.2006.03.005 (July 2006).
75. Walker, A. P. & Fodor, E. Interplay between Influenza Virus and the Host RNA Polymerase II Transcriptional Machinery. English. *Trends in Microbiology* **27.** Publisher: Elsevier, 398–407. doi:10.1016/j.tim.2018.12.013 (May 2019).
76. Core, L. J. *et al.* Defining the Status of RNA Polymerase at Promoters. English. *Cell Reports* **2.** Publisher: Elsevier, 1025–1035. doi:10.1016/j.celrep.2012.08.034 (Oct. 2012).
77. Noshi, T. *et al.* In vitro characterization of baloxavir acid, a first-in-class cap-dependent endonuclease inhibitor of the influenza virus polymerase PA subunit. *Antiviral Research* **160,** 109–117. doi:10.1016/j.antiviral.2018.10.008 (Dec. 2018).
78. Koppstein, D., Ashour, J. & Bartel, D. P. Sequencing the cap-snatching repertoire of H1N1 influenza provides insight into the mechanism of viral transcription initiation. eng. *Nucleic Acids Research* **43,** 5052–5064. doi:10.1093/nar/gkv333 (May 2015).
79. Izaurralde, E. *et al.* A nuclear cap binding protein complex involved in pre-mRNA splicing. English. *Cell* **78.** Publisher: Elsevier, 657–668. doi:10.1016/0092-8674(94)90530-4 (Aug. 1994).
80. Calero, G. *et al.* Structural basis of m7GpppG binding to the nuclear cap-binding protein complex. en. *Nature Structural Biology* **9.** Publisher: Nature Publishing Group, 912–917. doi:10.1038/nsb874 (Dec. 2002).
81. Schulze, W. M. & Cusack, S. Structural basis for mutually exclusive co-transcriptional nuclear cap-binding complexes with either NELF-E or ARS2. en. *Nature Communications* **8.** Publisher: Nature Publishing Group, 1302. doi:10.1038/s41467-017-01402-w (Nov. 2017).
82. Clark, M. P. *et al.* Discovery of a Novel, First-in-Class, Orally Bioavailable Azaindole Inhibitor (VX-787) of Influenza PB2. *Journal of Medicinal Chemistry* **57.** Publisher: American Chemical Society, 6668–6678. doi:10.1021/jm5007275 (Aug. 2014).
83. Tan, Y. H., Armstrong, J. A., Ke, Y. H. & Ho, M. Regulation of Cellular Interferon Production: Enhancement by Antimetabolites*. *Proceedings of the National Academy of Sciences* **67.** Publisher: Proceedings of the National Academy of Sciences, 464–471. doi:10.1073/pnas.67.1.464 (Sept. 1970).
84. Killip, M. J., Smith, M., Jackson, D. & Randall, R. E. Activation of the Interferon Induction Cascade by Influenza A Viruses Requires Viral RNA Synthesis and Nuclear Export. *Journal of Virology* **88.** Publisher: American Society for Microbiology, 3942–3952. doi:10.1128/jvi.03109-13 (Apr. 2014).
85. Donald, H. B. & Isaacs, A. Counts of Influenza Virus Particles. *Microbiology* **10.** Publisher: Microbiology Society, 457–464. doi:10.1099/00221287-10-3-457 (1954).
86. Saira, K. *et al.* Sequence Analysis of In Vivo Defective Interfering-Like RNA of Influenza A H1N1 Pandemic Virus. *Journal of Virology* **87.** Publisher: American Society for Microbiology, 8064–8074. doi:10.1128/jvi.00240-13 (July 2013).
87. Elshina, E. *et al. Influenza A virus transcription generates capped cRNAs that activate RIG-I* en. Pages: 2024.11.12.623191 Section: New Results. Nov. 2024. doi:10.1101/2024.11.12.623191.
88. Hoffmann, E., Neumann, G., Kawaoka, Y., Hobom, G. & Webster, R. G. A DNA transfection system for generation of influenza A virus from eight plasmids. eng. *Proceedings of the National Academy of Sciences of the United States of America* **97,** 6108–6113. doi:10.1073/pnas.100133697 (May 2000).
89. REED, L. & MUENCH, H. A SIMPLE METHOD OF ESTIMATING FIFTY PER CENT ENDPOINTS12. *American Journal of Epidemiology* **27,** 493–497. doi:10.1093/oxfordjournals.aje.a118408 (May 1938).
90. Gebhardt, A. *et al.* mRNA export through an additional cap-binding complex consisting of NCBP1 and NCBP3. en. *Nature Communications* **6.** Publisher: Nature Publishing Group, 8192. doi:10.1038/ncomms9192 (Sept. 2015).
91. Zajac, P., Islam, S., Hochgerner, H., Lönnerberg, P. & Linnarsson, S. Base preferences in non-templated nucleotide incorporation by MMLV-derived reverse transcriptases. eng. *PloS One* **8,** e85270. doi:10.1371/journal.pone.0085270 (2013).
92. Picelli, S. *et al.* Smart-seq2 for sensitive full-length transcriptome profiling in single cells. en. *Nature Methods* **10.** Publisher: Nature Publishing Group, 1096–1098. doi:10.1038/nmeth.2639 (Nov. 2013).

93. O'Connell, R. M. *et al.* Lentiviral Vector Delivery of Human Interleukin-7 (hIL-7) to Human Immune System (HIS) Mice Expands T Lymphocyte Populations. en. *PLoS ONE* **5,** e12009. doi:10.1371/journal.pone.0012009 (Aug. 2010).

94. Dadonaite, B. *et al.* A pseudovirus system enables deep mutational scanning of the full SARS-CoV-2 spike. English. *Cell* **186.** Publisher: Elsevier, 1263–1278.e20. doi:10.1016/j.cell.2023.02.001 (Mar. 2023).

95. Garcia-Beltran, W. F. *et al.* COVID-19-neutralizing antibodies predict disease severity and survival. eng. *Cell* **184,** 476–488.e11. doi:10.1016/j.cell.2020.12.015 (Jan. 2021).

Supplementary Figures

A

Replicate	Library	Reads	% of reads assigned to a guide	% of GeCKO gRNAs represented
1	Plasmid	35037970	74.7	96.1
	gDNA	34324456	66.9	94.7
	mRNA	30017765	67.4	64.7
2	Plasmid	30475752	73.5	99.7
	gDNA	39147617	66.0	97.9
	mRNA	65934508	64.5	60.8
3	Plasmid	31985045	74.5	99.4
	gDNA	27945288	66.4	97.4
	mRNA	31298994	65.6	57.4

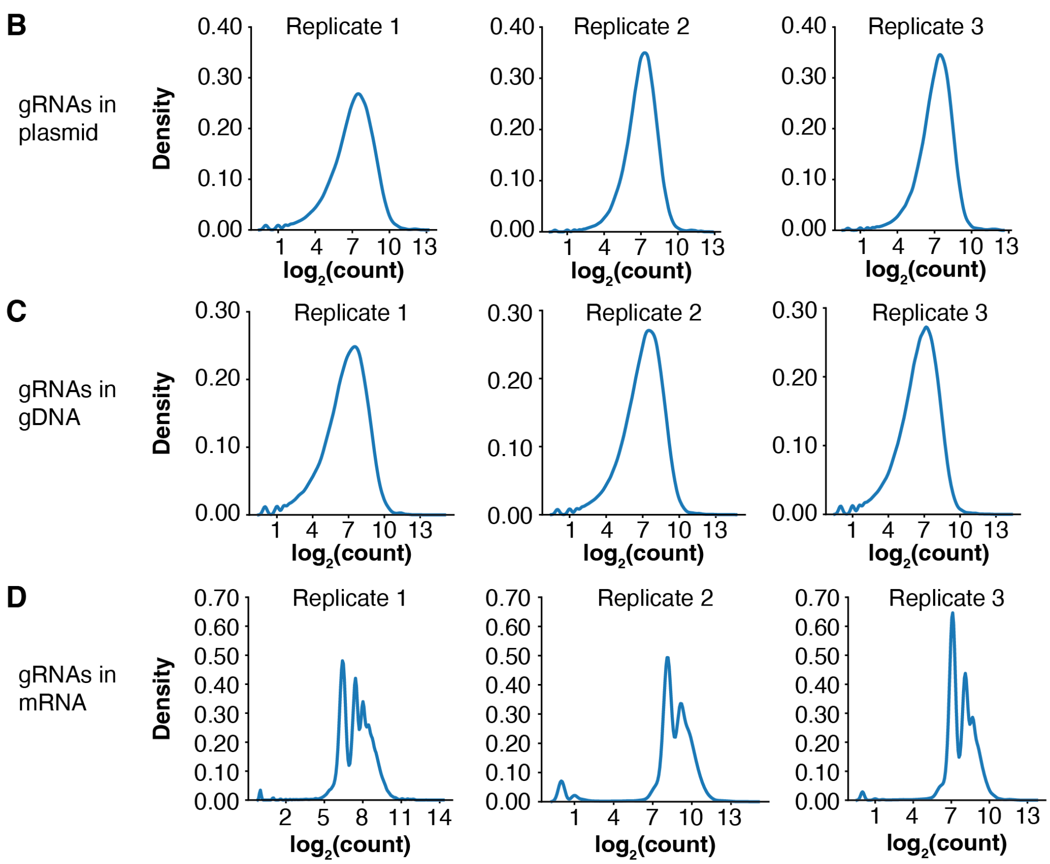

Supplementary Figure 1. Representation of GeCKO library gRNAs in CRITR-seq libraries, related to Figure 2.
(A) Three CRITR-seq libraries were generated by cloning the GeCKO library gRNA sequences into the CRITR-seq vector three independent times. Amplicon sequencing was performed on the region containing the gRNA in the plasmid library, the genomic DNA of the transduced A549 cells, and the mRNA from the transduced cells after 8 hour infection by $NS1_{mut}$. gRNAs were identified for reads matching the CRITR-seq vector for the 10 nucleotides upstream and 13 nucleotides downstream of the gRNA sequence, requiring perfect matching.
(B-D) Distribution of gRNAs by count in the plasmid (B), genomic DNA (C), and RNA (D) libraries.

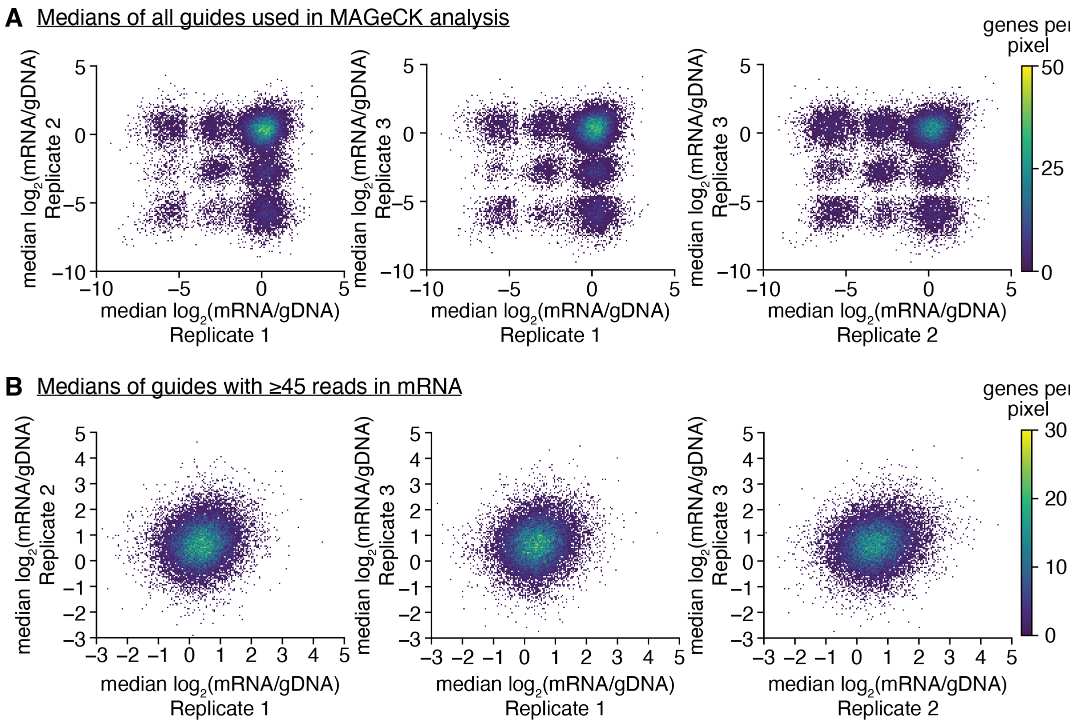

Supplementary Figure 2. Correlation plots between CRITR-seq screen replicates, related to Figure 2.

(A) MAGeCK analysis was performed on the subset of gRNAs with at least 25 reads in the gDNA in every replicate. In these graphs, genes are plotted based on the median $\log_2$ fold change of their targeting guides from each replicate. Color scale represents the density of the points in each pixel.

(B) To minimize noise from dropout, in each replicate we removed individual gRNAs with 45 or less reads in the mRNA before taking the median $\log_2$ fold change for each gene. The medians of the remaining guides are shown here. The correlation is still weak, indicating a high level of noise in the screen. However, these plots have less noise than those in (A), suggesting that dropout seems to be a significant contributor to the noise.

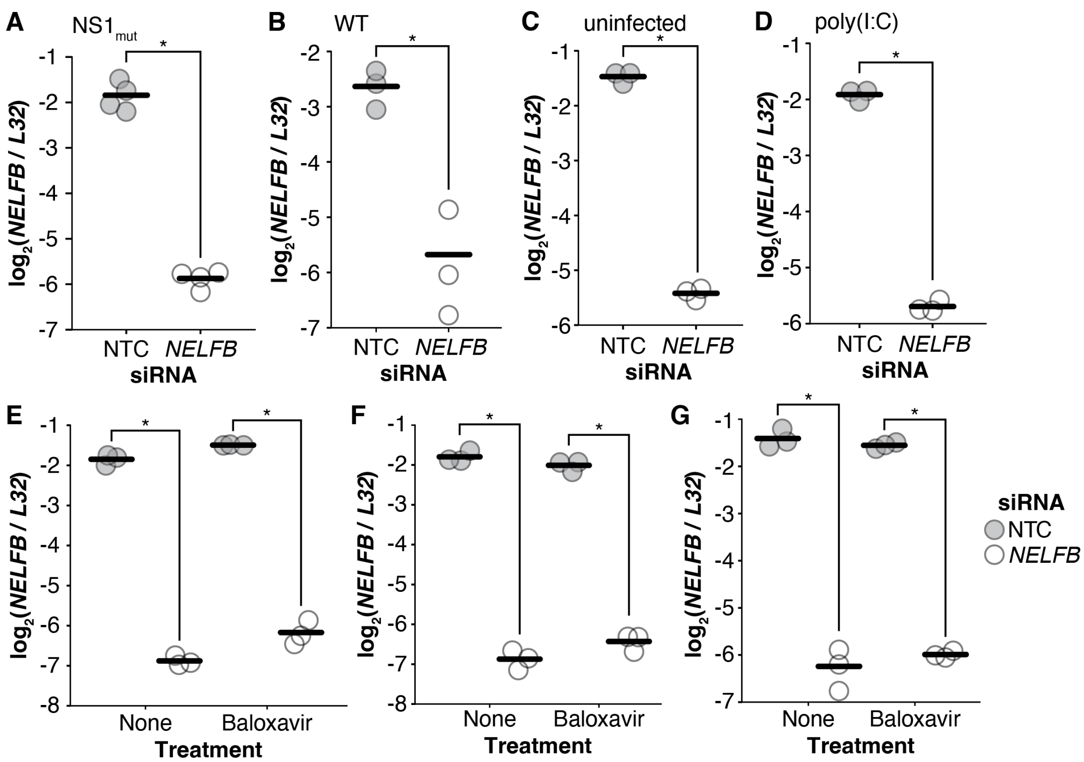

Supplementary Figure 3. Validation of *NELFB* knockdown by siRNA, related to Figures 3, 4, 5. (A-G) For each qPCR experiment after *NELFB* knockdown, we measured *NELFB* RNA levels to validate effectiveness of the siRNA treatment. RNA was taken from the same experiments as in Figures 3C and 4A-left (A); 3D and 4A-right (B); 3E (C); 3F(D); 4B (E); 5A-B (F); and 5C (G).
Biological replicates are shown as individual data point, with lines representing the means. Two-tailed t-tests were performed to compare *NELFB* knockdown with the non-targeting control in each condition. n=4 (A) or n=3 (B-F). * indicates $p<0.05$.

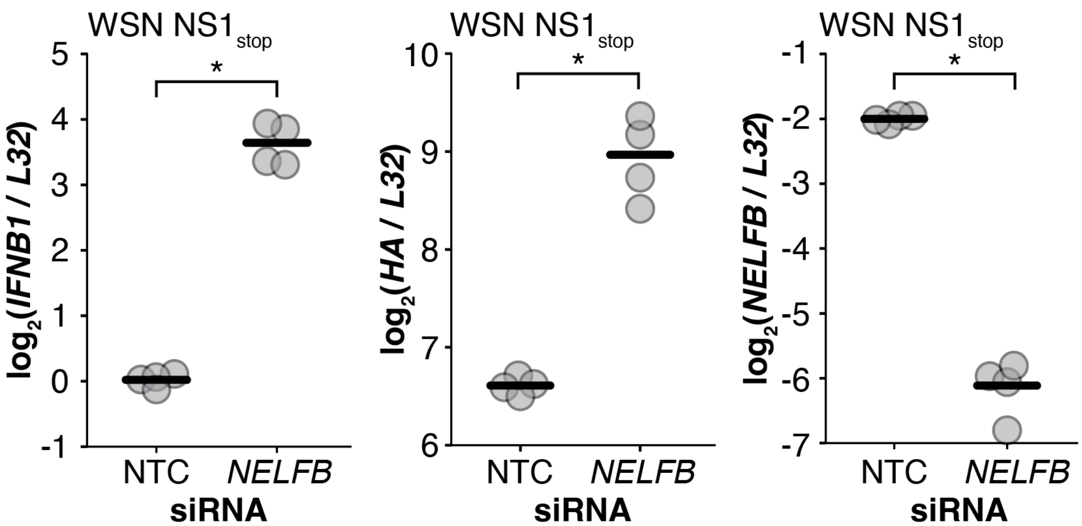

Supplementary Figure 4. Effects of *NELFB* knockdown on WSN NS1$_{\text{stop}}$ IAV, related to Figure 3, 4. The NS1$_{\text{mut}}$ virus used elsewhere in this study has the WSN genome segments 1-7 and PR8 segment 8 with early stop mutations in the NS1 open reading frame that do not affect the coding sequence of NS2. This virus was used for the CRITR-seq screen and most follow-up experiments because it grows to higher titers than the NS1$_{\text{stop}}$ virus in the fully WSN background. To validate the effects of *NELFB* are not particular to the NS1$_{\text{mut}}$ virus with mixed genetic background, we treated cells with either non-targeting control or *NELFB* siRNA for 9 days, followed by WSN NS1$_{\text{stop}}$ infection at an MOI of 1. RNA was harvested 8 hours post infection for qPCR analysis.
Biological replicates are shown as individual data points, with lines representing the means. Two-tailed t-tests were performed to compare *NELFB* knockdown with the non-targeting control in each condition. n=4, with two replicates each of two biological replicate viral populations. * indicates $p<0.05$.

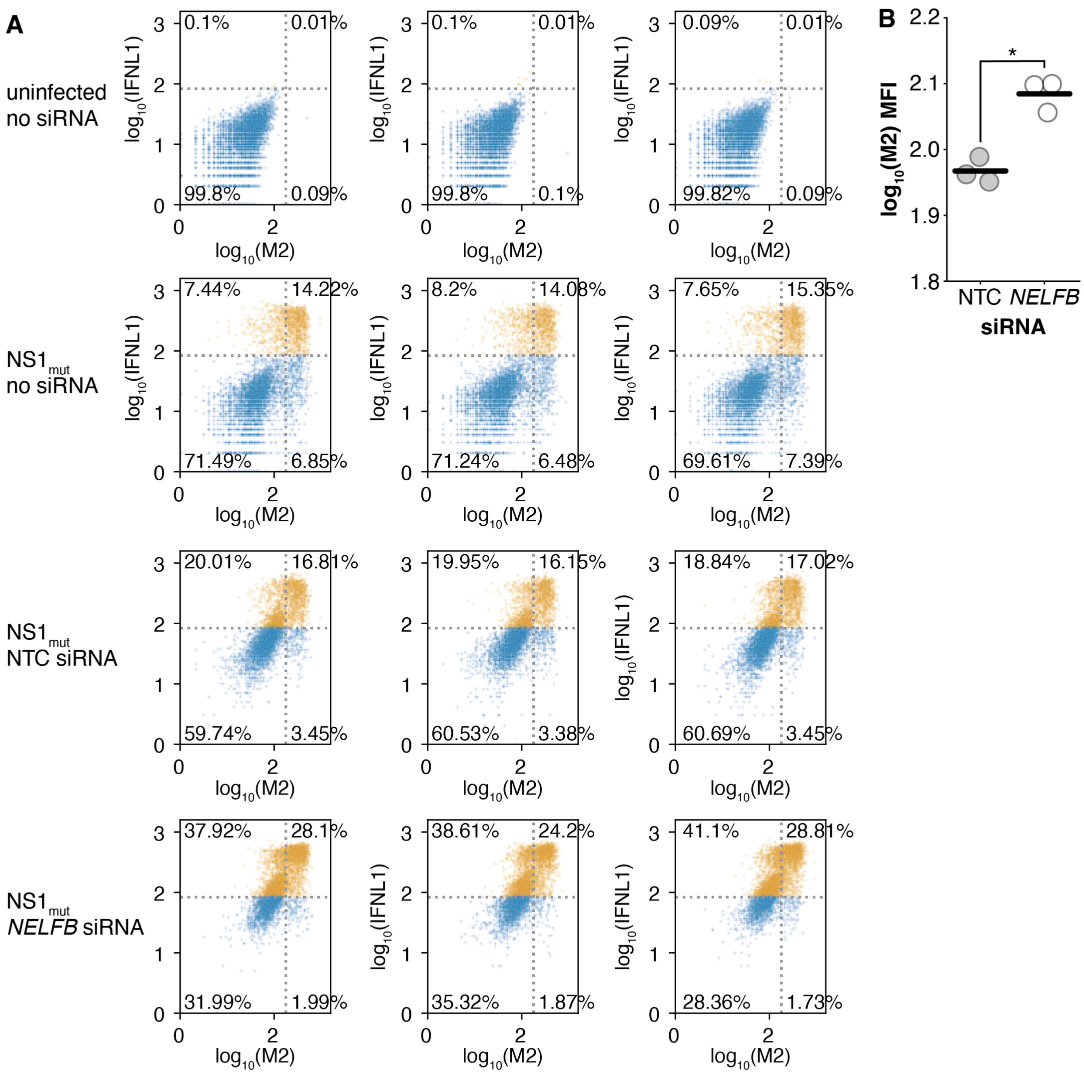

Supplementary Figure 5. Full flow cytometry data, related to Figures 4, 5.
A549 *IFNL1* reporter cells were treated for 9 days with siRNA and infected, or not, with NS1_{mut} at a genome-corrected MOI of 1. 13 hours post infection, cells were stained for the viral protein M2 and fixed for flow cytometry.
(A) Individual replicates shown. The threshold for IFNL1^{+} or M2^{+} cells was set at the fluorescence level for which an average of 0.1% of uninfected cells would be called as positive events. Interferon-positive events colored in orange. For visualization, data was subsetted to 5000 events to show equivalent numbers between conditions.
(B) Mean fluorescence intensity (MFI) of M2 staining. Two-tailed t-test was performed to compare targeted siRNA with the non-targeting control, n=3, * indicates $p<0.05$.

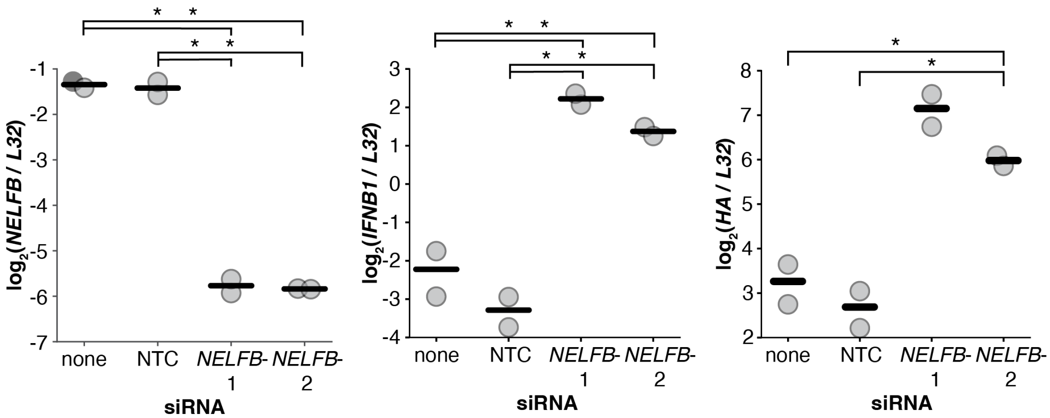

Supplementary Figure 6. qPCR validation of *NELFB* knockdown phenotype in RNA used for cap-length sequencing, related to Figure 4.
A549 cells were treated with either of 2 different *NELFB*-targeting siRNAs, a non-targeting control, or no siRNA, with 2 biological replicates per treatment. After 9 days of siRNA treatment, cells were infected with $NS1_{mut}$ at a genome-corrected MOI of 2. RNA was harvested 8 hours post infection for 5' RACE and sequencing (Figure 4C) and qPCR analysis. qPCR results shown here confirm *NELFB* knockdown and a consistent phenotype of increased viral RNA and interferon production in the samples treated with *NELFB* siRNA.
Biological replicates are shown as individual data points, with lines representing the means. Two-tailed t-tests were performed to compare each sample with the untreated condition and with the non-targeting control, n=2. * indicates $p<0.05$ after Benjamini-Hochberg multiple hypothesis correction.

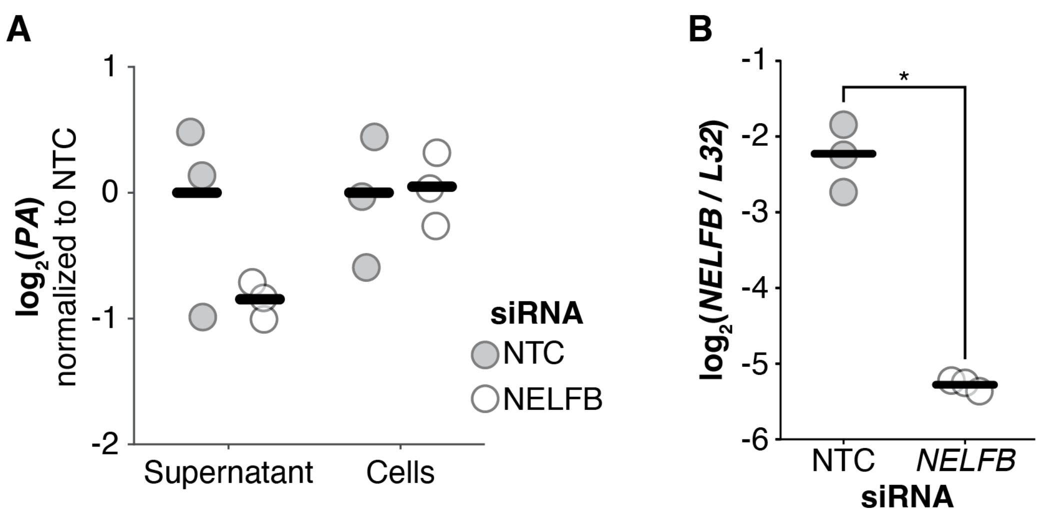

Supplementary Figure 7. *NELFB* knockdown does not increase viral titer, related to Figure 4.
(A-B) Same experiment as in Figure 4F, with different RNAs measured by qPCR. A549 cells were treated with siRNA for 9 days before infection with WT WSN at an infectious MOI of 5. Media was replaced with fresh IGM 2 hours post infection. 14 hours post infection, viral supernatant was collected and cells were lysed for RNA extraction of both. Reverse transcription was performed using universal influenza primers for the RNA from the supernatant, and random hexamer primers for the RNA from the cell lysate.
Biological replicates are shown as individual data points, with lines representing the means. Two-tailed t-tests were performed to compare targetign siRNA with the non-targeting control, n=3. Benjamini-Hochberg multiple hypothesis correction was performed for panel A. * indicates $p<0.05$.

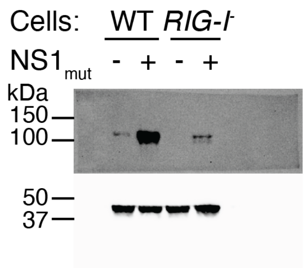

Supplementary Figure 8. RIG-I protein expression in clonal *RIG-I* knockout A549 cell line, related to Figure 5.

We transfected A549 cells with Cas9 ribonucleoprotein using a gRNA targeting *RIG-I*. After performing dilution cloning to isolate single cells, the clonal-derived line was infected with $NS1_{mut}$ at a genome-corrected MOI of 2 for 24 hours. Infected and uninfected A549 or A549 RIG-I knockout cells were lysed for SDS-PAGE and Western blot.

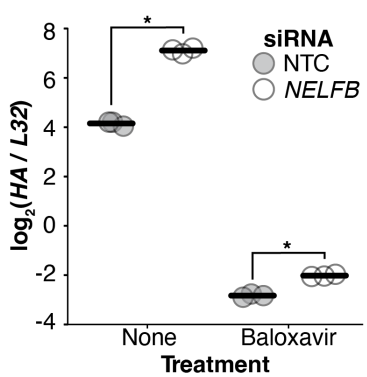

Supplementary Figure 9. *RIG-I* knockout does not affect *HA* RNA levels, related to Figure 5.

Same experiment as in Figure 5C, but measuring *HA* levels by qPCR. A *RIG-I* knockout cell line derived from a single cell clone (Figure S8) was treated with siRNA for 9 days. Cells were infected with $NS1_{mut}$ at a genome-corrected MOI of 1, with or without 100 nM baloxavir acid added at time of infection. RNA was harvested 8 hours post infection for qPCR analysis.

Points represent biological replicates, with lines indicating the means. Two-tailed t-tests were performed comparing the NELFB siRNA samples with the non-targeting control for each treatment condition, n=3. * indicates $p<0.05$ after Benjamini-Hochberg multiple hypothesis correction.